

**THE INTRINSIC DERIVATIVE AND CENTRIFUGAL FORCES
IN GENERAL RELATIVITY: II. APPLICATIONS
TO CIRCULAR ORBITS IN SOME FAMILIAR
STATIONARY AXISYMMETRIC SPACETIMES**

DONATO BINI

*Istituto per Applicazioni della Matematica C.N.R., I-80131 Napoli, Italy and
International Center for Relativistic Astrophysics, University of Rome, I-00185 Roma, Italy*

PAOLO CARINI*

*GP-B, Hansen Labs, Stanford University, Stanford, CA 94305, USA and
International Center for Relativistic Astrophysics, University of Rome, I-00185 Roma, Italy*

ROBERT T. JANTZEN

*Department of Mathematical Sciences, Villanova University, Villanova, PA 19085, USA and
International Center for Relativistic Astrophysics, University of Rome, I-00185 Roma, Italy*

Received 17 December 1996

The tools developed in a preceding article for interpreting spacetime geometry in terms of all possible space-plus-time splitting approaches are applied to circular orbits in some familiar stationary axisymmetric spacetimes. This helps give a more intuitive picture of their rotational features including spin precession effects, and puts related work of Abramowicz, de Felice, and others on circular orbits in black hole spacetimes into a more general context.

Keywords: gravitoelectromagnetism–inertial forces

1. Introduction

“Rotating spacetimes” have captured people’s imaginations ever since “rigid” rotations in Minkowski spacetime were considered within the theory of general relativity. Even this simple example which is the foundation of the “fictitious” centrifugal and Coriolis forces in classical physics has led to its share of confusion about rotation in relativity. Gödel’s discovery¹ of the spacetime which bears his name certainly added fuel to the fire, which was again stoked by the discovery of the rotating black hole solution of Kerr² and its generalizations.^{3,4}

The language of gravitoelectromagnetism,⁵ specialized in the preceding companion article⁶ (to be referred to here as [BCJ1]) for stationary axially symmetric spacetimes, helps us to understand the effects of rotation as well as those of acceleration and spatial curvature in these three classic spacetime examples. Indeed the lines of force of the various gravitoelectromagnetic vector fields, especially in the

* Present Address: Physics Department, Amherst College, Amherst, MA 01002, USA.

Kerr spacetimes, help give a more tangible way of interpreting the behavior of test particle motions in the gravitational field of these spacetimes.

Here we focus on the simpler case of circular orbits following Killing trajectories in these spacetimes, confining our attention to the equatorial plane in the Kerr spacetimes.^{7,9} This test particle motion is an example of “purely transverse” relative acceleration.¹⁰ By exploring the roles played by the radial spatial gravitational forces, one obtains a clearer picture of the action and interrelationships of the various gravitoelectric (GE), gravitomagnetic (GM), and space curvature (SC) forces that one may define within each spacetime as well as of the correspondences one may establish between these different spacetimes. Presenting the details of these applications also helps make more concrete the somewhat abstract but powerful language of gravitoelectromagnetism itself, which can be valuable in interpreting the geometry of other spacetimes. In particular, previous discussions of circular orbits in black hole spacetimes by Abramowicz, de Felice, and others^{11–34} are fit into a more general picture which helps to clarify their particular analyses of the behavior of certain properties of these orbits.

Each of these three classes of spacetimes have natural stationary axisymmetric nonlinear reference frames, i.e., threaded slicings (hypersurface foliations with transversal congruences of curves) of the spacetime which are adapted to two Killing vector fields associated with a 2-dimensional stationary axisymmetry group. The nonlinear reference frames for the rotating Minkowski and Gödel spacetimes have an additional translational symmetry making them cylindrically symmetric as well. In each case the threading and slicing families of test observers associated with these nonlinear reference frames are tied to the geometry of the spacetime and help elucidate its properties.

In the case of Kerr, the nonlinear reference frame associated with Boyer-Lindquist coordinates $\{t, r, \theta, \phi\}$ ³⁸ has as its threading observers (following the time coordinate line Killing trajectories) the distantly nonrotating observers or static observers, while the slicing observers (moving normal to the time coordinate hypersurfaces) are the locally nonrotating observers or zero-angular-momentum observers. Both observer families are accelerated, the threading observers opposing the dragging along action of the rotating black hole, while the slicing observers are dragged along by the hole with respect to spatial infinity. In the Gödel spacetime, the nonlinear reference frame of cylindrical coordinates $\{t, \rho, \phi, z\}$ has the threading observers moving along the geodesic flow lines of the rotating dust source, while the accelerated slicing observers oppose the global rotation of the spacetime. In the rotating Minkowski spacetime, the accelerated threading observers are uniformly rotating, while the geodesic slicing observers are a global family of inertial observers associated with the usual time lines of an orthonormal Cartesian coordinate system. Each of these three spacetime examples exhibits different configurations of the various gravitoelectromagnetic fields whose comparison offers insights about the nature of the spacetimes themselves.

The Gödel spacetime was first studied as an example of a constant gravitomag-

netic field configuration by Wilkins and Jacobs,³⁹ based on the analogy between linearized general relativity and electromagnetism.⁴⁰ Their pioneering work stimulated the present program of trying to better understand fully nonlinear general relativity in terms of observer-splittings.

2. Gravitoelectromagnetic potentials, fields, and forces

The “rotating Minkowski” spacetime is just Minkowski spacetime expressed in terms of the nonlinear reference frame associated with a family of uniformly rotating test observers (threading) and the time hypersurfaces (slicing) associated with the global inertial Cartesian coordinates with respect to which this rotation takes place. It is most easily described in terms of rotating cylindrical coordinates $\{t, \rho, \phi, z\}$, where $\phi = \phi' - \Omega t$ gives the relationship to the nonrotating angular coordinate ϕ' , as discussed by Landau and Lifshitz⁴¹ and in [BCJ1]. Although the coordinate angular velocity Ω about the z -axis may take any real value (define $\mathcal{R} = 1/|\Omega|$), here it will be assumed to be positive in order to discuss corotation and counter-rotation with respect to the sense defined by the positive z -axis and the righthand rule.

The Gödel spacetime is a solution of the Einstein equations with constant dust energy density $\rho_{(0)}$ and cosmological constant Λ related by $\Lambda = -\Omega^2 = -(2\mathcal{R}^2)^{-1} = -4\pi\rho_{(0)}$, where $\mathcal{R} = |\sqrt{2}\Omega|^{-1}$ is Gödel’s curvature parameter “ a ” and Ω is the nonzero constant parametrizing the constant vorticity of the fluid source. Although it may take any nonzero value, it will be assumed to be positive here for the same reason as above, so that the threading observers corotate with respect to the positive z -axis in the cylindrical coordinates used here. These coordinates differ from others in the literature by a rescaling, chosen so that to linear order in the vorticity parameter Ω the Gödel and rotating Minkowski metrics are the same, although important differences occur at second order. In these coordinates the limiting behavior approaching the axis of symmetry of the associated nonlinear reference frame is also the same to lowest order in this parameter, and the limit of both metrics as $\Omega \rightarrow 0$ is just Minkowski spacetime expressed in nonrotating cylindrical coordinates. Thus the new parametrization of the Gödel metric emphasizes the key feature of its geometry, namely the global rotation, rather than the related spatial curvature.

The Kerr spacetime describes the geometry around a rotating black hole with mass \mathcal{M} (directly defining a length scale \mathcal{R}) and angular momentum per unit mass a as seen from infinity. The angular velocity parameter a will be assumed positive as above, so that all three spacetime examples rotate in the same sense. The limit $a = 0$ gives the nonrotating Schwarzschild spacetime, while $a = \mathcal{M}$ is the “extreme Kerr” case. The usual Boyer-Lindquist coordinates $\{t, r, \theta, \phi\}$ will be used here.

In each spacetime the Killing vector field $e_0^\alpha = \delta^\alpha_t$ generates the stationary symmetry while the spacelike Killing vector field δ^α_ϕ generates the axisymmetry, and the spatial coordinates are orthogonal. For uniformity of discussion, the radial Kerr coordinate symbol r will be used to denote the cylindrical coordinate ρ in the other two examples as well, while the physical (orthonormal) component along $-\delta^\alpha_\theta$ perpendicular to the equatorial plane in Kerr will be referred to as along the

positive z -axis as in the case of the plane $z = 0$ in the other spacetimes and will be indicated by the index \hat{z} . The latter plane will be referred to as the equatorial plane in all cases. For graphing purposes it is natural to introduce the rescaled radial variable $\bar{r} = r/\mathcal{R}$ for all these spacetimes and $\bar{a} = a/\mathcal{R} = a/\mathcal{M}$ for the additional parameter in the Kerr case.

For all the three spacetimes under consideration, the spacetime metric restricted to the world sheet of this plane can be expressed in the reference (i.e., coordinate), threading, and slicing decompositions respectively as

$$\begin{aligned} ds^2 &= {}^{(4)}g_{tt}dt^2 + 2{}^{(4)}g_{t\phi}dtd\phi + {}^{(4)}g_{\phi\phi}d\phi^2 + {}^{(4)}g_{rr}dr^2 \\ &= -M^2(dt - M_\phi d\phi)^2 + \gamma_{\phi\phi}d\phi^2 + \gamma_{rr}dr^2 \\ &= -N^2dt^2 + g_{\phi\phi}(d\phi + N^\phi dt)^2 + g_{rr}dr^2 . \end{aligned} \quad (2.1)$$

Since the threading and slicing observer-adapted frames associated with this adapted coordinate system are obtained by projection of the coordinate frame, their spatial structure functions vanish. Table 1 gives the expressions of the various threading and slicing quantities for the three cases.

Table 1. The lapse, and the nonzero observer-adapted components of the shift and spatial metric in both the threading and slicing points of view are given for the rotating Minkowski, Gödel and Kerr spacetimes on the equatorial plane. Note the Gödel parameter relation $\sqrt{2}|\Omega| = 1/\mathcal{R}$ useful for reinterpreting quantities in terms of spatial curvature rather than vorticity.

lapse, shift and spatial metric	Rotating Minkowski	Gödel	Kerr
$N = (-{}^{(4)}g^{00})^{-1/2}$	1	$c/\sqrt{1-s^2}$	$\sqrt{r\Delta/(r^3 + a^2r + 2a^2\mathcal{M})}$
$N^\phi = N_\phi/g_{\phi\phi}$	Ω	$\Omega/(1-s^2)$	$-2a\mathcal{M}/(r^3 + a^2r + 2a^2\mathcal{M})$
$N_\phi = {}^{(4)}g_{0\phi}$	Ωr^2	$2s^2/\Omega$	$-2a\mathcal{M}/r$
$g_{\phi\phi} = {}^{(4)}g_{\phi\phi}$	r^2	$2s^2(1-s^2)/\Omega^2$	$(r^3 + a^2r + 2a^2\mathcal{M})/r$
$g_{rr} = \gamma_{rr} = {}^{(4)}g_{rr}$	1	1	r^2/Δ
$M = (-{}^{(4)}g_{00})^{1/2}$	γ^{-1}	1	$\sqrt{(r-2\mathcal{M})/r}$
$M_\phi = -{}^{(4)}g_{0\phi}/{}^{(4)}g_{00}$	$\Omega r^2 \gamma^2$	$2s^2/\Omega$	$-2a\mathcal{M}/(r-2\mathcal{M})$
$\gamma_{\phi\phi} = {}^{(4)}g_{\phi\phi} - ({}^{(4)}g_{0\phi})^2/{}^{(4)}g_{00}$	$\gamma^2 r^2$	$2s^2 c^2/\Omega^2$	$r\Delta/(r-2\mathcal{M})$

$$\begin{aligned} \gamma &\equiv (1 - \Omega^2 r^2)^{-1/2}, \quad s \equiv \sinh(\sqrt{2}\Omega r/2), \quad c \equiv \cosh(\sqrt{2}\Omega r/2), \quad t \equiv \tanh(\sqrt{2}\Omega r/2), \\ S &\equiv \sinh(\sqrt{2}\Omega r), \quad C \equiv \cosh(\sqrt{2}\Omega r), \quad T \equiv \tanh(\sqrt{2}\Omega r), \quad \Delta \equiv r^2 - 2\mathcal{M}r + a^2, \end{aligned}$$

The general formulas of [BCJ1] for constant speed test particle circular orbits in stationary axisymmetric spacetimes are easily evaluated for the present explicit metrics. The test particle moves along the ϕ direction with constant speed. The 4-velocity of a nonzero rest mass test particle is parametrized by the coordinate angular velocity $\zeta = \dot{\phi} = d\phi/dt$ as follows

$$U^\alpha = \Gamma[\delta^\alpha_t + \zeta \delta^\alpha_\phi], \quad (2.2)$$

where $\Gamma = dt/d\tau_U > 0$ is defined by

$$\begin{aligned}\Gamma^{-2} &= -[{}^{(4)}g_{tt} + 2\zeta{}^{(4)}g_{t\phi} + \zeta^2{}^{(4)}g_{\phi\phi}] = -{}^{(4)}g_{\phi\phi}(\zeta - \zeta_-)(\zeta - \zeta_+) \\ &= M^2(1 - M_\phi\zeta)^2 - \gamma_{\phi\phi}\zeta^2 = N^2 - g_{\phi\phi}(\zeta + N^\phi)^2\end{aligned}\quad (2.3)$$

and τ_U is a proper time parametrization of the world line. The timelike condition for the 4-velocity U^α requires $\Gamma^{-2} > 0$, constraining ζ to belong to the interval $[\zeta_-, \zeta_+]$ between the roots of the quadratic equation $\Gamma^{-2} = 0$ in ζ corresponding to null directions, namely

$$\begin{aligned}\zeta_\pm &= [{}^{(4)}g_{t\phi} \pm ({}^{(4)}g_{t\phi}^2 - g_{\phi\phi}g_{tt})^{1/2}] / {}^{(4)}g_{\phi\phi} \\ &= [-M^2M^\phi \pm M\gamma_{\phi\phi}^{-1/2}] / (1 - M^2M_\phi M^\phi) = -N^\phi \pm N(g_{\phi\phi})^{-1/2} .\end{aligned}\quad (2.4)$$

The 4-velocity of a zero rest mass particle (for which $\Gamma^{-2} = 0$) has an arbitrary normalization factor $\Gamma_{(\text{null})}$ in place of Γ in equation (2.2)

$$P_\pm^\alpha = \Gamma_{(\text{null})}[\delta^\alpha_t + \zeta_\pm \delta^\alpha_\phi] .\quad (2.5)$$

Circular orbits for which $\zeta \geq 0$ or $\zeta < 0$ will be referred to respectively as corotating or counter-rotating (with respect to the nonlinear reference frame or the threading observers).

Note that the coordinate angular velocity of the slicing observers is just the average of the two limiting angular velocities

$$\zeta_{(\text{sl})} = \zeta_{(\text{nmp})} = (\zeta_- + \zeta_+)/2 = -N^\phi ,\quad (2.6)$$

which is just equation (33.16) of Misner, Thorne, and Wheeler³⁸ in the specific context of the Kerr spacetime. Their exercise (33.3) following the discussion of Bardeen⁴² applies to the general (orthogonally transitive) stationary axially symmetric case,⁴³ so that one may interpret the slicing observers as the locally nonrotating observers with respect to the Sagnac effect. They experience no Sagnac effect for the oppositely directed accelerated photons constrained by mirrors or fiber optical cable to remain on a given circular orbit, meaning that the alternating meeting points of these photons lie on the same observer world line. They are also called the “zero angular momentum observers” (ZAMO’s) since they are orthogonal to the angular Killing vector and therefore have vanishing angular momentum. A complementary formula exists for the angular coordinate component of the threading shift 1-form

$$M_\phi = (\zeta_-^{-1} + \zeta_+^{-1})/2 .\quad (2.7)$$

This is related to the Sagnac effect as well, as explained below.

The physical components of the velocities measured by the threading and slicing observers for such motion are related to the coordinate angular velocity by linear or fractional linear transformations

$$\nu(U, m)^{\hat{\phi}} = \gamma_{\phi\phi}^{1/2}\zeta/[M(1 - M_\phi\zeta)] , \quad \nu(U, n)^{\hat{\phi}} = g_{\phi\phi}^{1/2}(\zeta + N^\phi)/N\quad (2.8)$$

and

$$\begin{aligned}\zeta &= M\nu(U, m)^{\hat{\phi}}/[\gamma_{\phi\phi}^{1/2} + MM_{\phi}\nu(U, m)^{\hat{\phi}}] \\ &= -N^{\phi} + Ng_{\phi\phi}^{-1/2}\nu(U, n)^{\hat{\phi}}.\end{aligned}\tag{2.9}$$

Note that when the shift is nonzero, test particle motions with angular velocities of equal magnitude but opposite sign lead to physical velocities which do not have the same magnitude and vice versa. When $\nu(U, u)^{\hat{\phi}} = \pm 1$, the latter equation reduces to Eq. (2.4).

The ‘‘coordinate’’ gamma factor is easily expressed in terms of the usual Lorentz gamma factor associated with these relative velocities

$$\begin{aligned}\Gamma &= \gamma(U, m)/[M(1 - M_{\phi}\zeta)] \equiv \Gamma(U, m) \\ &= \gamma(U, n)/N \equiv \Gamma(U, n).\end{aligned}\tag{2.10}$$

These formulas may be used to express the angular momentum (per unit mass)

$$p_{\phi} = U_{\phi} = \Gamma\nu(U, n)_{\phi} = g_{\phi\phi}\Gamma(\zeta - \zeta_{(\text{sl})})\tag{2.11}$$

of U defined by the rotational Killing vector δ^{α}_{ϕ} and its Killing energy (per unit mass) $\mathcal{E} = -U_t = M^{-1}\gamma(U, m)$ defined by the Killing vector δ^{α}_t , both conserved for geodesic motion. These are related to the coordinate gamma factor by the identity $-1 = U_{\alpha}U^{\alpha} = \Gamma(-\mathcal{E} + \zeta p_{\phi})$ in the timelike case and $0 = P_{\alpha}P^{\alpha} = \Gamma_{(\text{null})}(-\mathcal{E} + \zeta P_{\phi})$ in the null case, where $\mathcal{E} = -P_t$. Note that the slicing relative velocity is directly proportional to the angular momentum.

In the timelike case the ratio

$$\bar{\zeta} = \frac{\mathcal{E}}{p_{\phi}} = -\frac{g_{tt} + \zeta g_{\phi t}}{g_{t\phi} + \zeta g_{\phi\phi}}\tag{2.12}$$

defines the angular velocity of the spacelike circular orbit orthogonal to U^{α} with unit tangent $\bar{U}^{\alpha} = \bar{\Gamma}(\delta^{\alpha}_t + \bar{\zeta}\delta^{\alpha}_{\phi})$, $\bar{\Gamma} > 0$ and having the same sense of rotation. This is the angular direction of the local rest space of the test particle.

Consider only a nonzero rest mass test particle in what follows. The various spatial forces acting on such a particle all point along the radial direction whether expressed in the threading or in the slicing observer-adapted frame. In the ‘‘spatial equation of motion’’ (9.9) of [BCJ1], the Lie total spatial covariant derivative of the spatial momentum reduces to minus the space curvature force (see equations (12.7) and (12.23) of [BCJ1]) and one finds the following simple results for the equation of motion in the threading, hypersurface, and slicing points of view respectively

$$\begin{aligned}-F(U, u)^{\hat{r}} &= F_{(\text{lie})}^{(\text{G})}(U, u)^{\hat{r}} + F^{(\text{SC})}(U, u)^{\hat{r}}, \quad u = m, n, \\ -F(U, n)^{\hat{r}} &= F_{(\text{lie})}^{(\text{G})}(U, n, e_0)^{\hat{r}} + F^{(\text{SC})}(U, n, e_0)^{\hat{r}},\end{aligned}\tag{2.13}$$

namely, minus the relative non-gravitational spatial force must balance the sum of the Lie spatial gravitational force and the space curvature force. The spatial gravitational forces in the various points of view can be separated into their gravito-electric (GE), vector gravitomagnetic (GM), and symmetric tensor gravitomagnetic

expansion (EX) components

$$\begin{aligned}
 F_{(\text{lie})}^{(\text{G})}(U, m)^{\hat{r}} &= \gamma(U, m)[g(m)^{\hat{r}} + \nu(U, m)^{\hat{\phi}} H(m)^{\hat{z}}] \\
 &= F^{(\text{GE})}(U, m)^{\hat{r}} + F^{(\text{GM})}(U, m)^{\hat{r}} , \\
 F_{(\text{lie})}^{(\text{G})}(U, n)^{\hat{r}} &= \gamma(U, n)[g(n)^{\hat{r}} - 2\nu(U, n)^{\hat{\phi}} \theta(n)_{\hat{r}\hat{\phi}}] \\
 &= F^{(\text{GE})}(U, n)^{\hat{r}} + F^{(\text{EX})}(U, n)^{\hat{r}} , \\
 F_{(\text{lie})}^{(\text{G})}(U, n, e_0)^{\hat{r}} &= \gamma(U, n)[g(n)^{\hat{r}} + \frac{1}{2}\nu(U, n)^{\hat{\phi}} H(n, e_0)^{\hat{z}} - \nu(U, n)^{\hat{\phi}} \theta(n)_{\hat{r}\hat{\phi}}] \\
 &= F^{(\text{GE})}(U, n)^{\hat{r}} + F^{(\text{GM})}(U, n, e_0)^{\hat{r}} + F^{(\text{EX})}(U, n, e_0)^{\hat{r}} ,
 \end{aligned} \tag{2.14}$$

where the sum of terms defines respectively the individually named force terms. The space curvature forces reduce simply to the sign-reversal of $\gamma(U, u)$ times the Lie relative centripetal acceleration

$$\begin{aligned}
 F^{(\text{SC})}(U, m)^{\hat{r}} &= -\kappa(\phi, m)^{\hat{r}} \gamma(U, m) |\nu(U, m)^{\hat{\phi}}|^2 , \\
 F^{(\text{SC})}(U, n)^{\hat{r}} &= -\kappa(\phi, n)^{\hat{r}} \gamma(U, n) |\nu(U, n)^{\hat{\phi}}|^2 , \\
 F^{(\text{SC})}(U, n, e_0)^{\hat{r}} &= -\kappa(\phi, n)^{\hat{r}} \gamma(U, n) [\nu(U, n)^{\hat{\phi}}] [\nu(U, n)^{\hat{\phi}} - \nu(e_0, n)^{\hat{\phi}}] ,
 \end{aligned} \tag{2.15}$$

where

$$\kappa(\phi, m)^{\hat{r}} = -(\ln \gamma_{\phi\phi}^{1/2})_{,\hat{r}} , \quad \kappa(\phi, n)^{\hat{r}} = -(\ln g_{\phi\phi}^{1/2})_{,\hat{r}} \tag{2.16}$$

are the signed Lie relative curvatures of the ϕ coordinate lines in the threading and hypersurface points of view and

$$\nu(e_0, n)^{\hat{\phi}} = N^{-1} N^{\hat{\phi}} = (g_{\phi\phi})^{1/2} N^{-1} N^{\phi} \tag{2.17}$$

is the physical component $\nu(m, n)^{\hat{\phi}}$ along the positive ϕ direction of the relative velocity of the threading observers with respect to the slicing observers when e_0^α is timelike, and of the relative velocity of the time coordinate lines in general. The caret index notation indicates physical (orthonormal) components along the orthogonal coordinate frame vectors in the slicing point of view and along their corresponding spatially projected vectors of the associated orthogonal observer-adapted spatial frame in the threading point of view.

Finally, the nonzero components of the gravitoelectric and gravitomagnetic vector fields together with the expansion can be calculated from their expressions in the observer adapted frames (see equations (14.5) and (14.6) of [BCJ1])

$$\begin{aligned}
 g(m)_r &= (\gamma_{rr})^{1/2} g(m)_{\hat{r}} = -(\ln M)_{,r} , \\
 g(n)_r &= (g_{rr})^{1/2} g(n)_{\hat{r}} = -(\ln N)_{,r} , \\
 H(m)^z &= H(m)^{\hat{z}} = M(\gamma_{rr}\gamma_{\phi\phi})^{-1/2} M_{\phi,r} , \\
 H(n, e_0)^z &= H(n, e_0)^{\hat{z}} = N^{-1}(g_{rr}g_{\phi\phi})^{-1/2} N_{\phi,r} , \\
 \theta(n)_{r\phi} &= (g_{\phi\phi}g_{rr})^{1/2} \theta(n)_{\hat{r}\hat{\phi}} = -(1/2)g_{\phi\phi} N^{-1} N^{\phi}_{,r} .
 \end{aligned} \tag{2.18}$$

Table 2. Causal restrictions, spatial gravitational force field quantities, and geodesic and null conditions for circular orbits in the rotating Minkowski and Gödel spacetimes.

	Rotating Minkowski	Gödel
length scale \mathcal{R}	Ω^{-1}	$ \sqrt{2}\Omega ^{-1}$
threading region of validity	$r < r_{(h)} = \Omega^{-1}$	everywhere
slicing region of validity	everywhere	$r < r_{(h)} = \mathcal{R} \operatorname{arcsinh} 1$
$\nu(m, n)^{\hat{\phi}} = -\nu(n, m)^{\hat{\phi}}$	Ωr	$\sqrt{2} t$
gravitoelectric field	$g(m)^{\hat{r}} = \gamma^2 \Omega^2 r > 0$ $g(n)^{\hat{r}} = 0$	$g(m)^{\hat{r}} = 0$ $g(n)^{\hat{r}} = -\frac{\sqrt{2}\Omega t}{1-s^2} < 0$
gravitomagnetic field	$H(m)^{\hat{z}} = 2\Omega\gamma^2 > 0$ $H(n, e_0)^{\hat{z}} = 2\Omega$	$H(m)^{\hat{z}} = 2\Omega > 0$ $H(n, e_0)^{\hat{z}} = 2\Omega > 0$
expansion	$\theta(n)_{\hat{r}\hat{\phi}} = 0$	$\theta(n)_{\hat{r}\hat{\phi}} = -\frac{\Omega s^2}{1-s^2} < 0$
signed relative curvature	$\kappa(\phi, m)^{\hat{r}} = -\frac{2}{r} < 0$ $\kappa(\phi, n)^{\hat{r}} = -\frac{1}{r} < 0$	$\kappa(\phi, m)^{\hat{r}} = -\sqrt{2}\Omega T^{-1}$ $\kappa(\phi, n)^{\hat{r}} = -\frac{\sqrt{2}\Omega(1-2s^2)}{2t(1-s^2)}$
counter-rotating and co-rotating timelike geodesics	$\phi_- = -\Omega$ $\nu(U_-, m)^{\hat{\phi}} = -\Omega r$ $\nu(U_-, n)^{\hat{\phi}} = 0$	$\phi_{\pm} = -\frac{2\Omega}{1-2s^2}, 0$ $\nu(U_{\pm}, m)^{\hat{\phi}} = -\sqrt{2} T, 0$ $\nu(U_{\pm}, n)^{\hat{\phi}} = -\frac{\sqrt{2}t}{1-2s^2}, \sqrt{2} t$
null orbits	$\zeta_{\pm} = -\Omega \pm 1/r$	$\zeta_{\pm} = \frac{\Omega}{1-s^2} [-1 \pm t^{-1}/\sqrt{2}]$

Explicit expressions for all of these quantities in the various points of view are given in Tables 2 and 3 for each of the three spacetimes under consideration.

The threading point of view is valid for those points of spacetime where the threading is timelike, i.e., where ${}^{(4)}g_{tt} < 0$ (or $M > 0$), while the hypersurface/slicing points of view are valid where the slicing is spacelike, or equivalently where the normal to the slicing is timelike, i.e., where ${}^{(4)}g^{tt} < 0$ (or $N > 0$). If the threading observers become spacelike in a region where the slicing observers are still timelike, then the threading point of view is still valid where the magnitude of the relative velocity of the threading observers with respect to the slicing observers is $|\nu(m, n)^{\hat{\phi}}| = |N^{-1}N^{\hat{\phi}}| < 1$. Vice versa, if the slicing observers become spacelike in a region where the threading observers are still timelike, then the slicing point of view is still valid in the region where $|\nu(n, m)^{\hat{\phi}}| < 1$. The regions of validity of the threading and slicing points of view are given in Tables 2 and 3.

For both the rotating Minkowski and Gödel spacetimes, the magnitude of the relative velocity is an increasing function of r which leads to the existence of an outer light cylinder at $r = r_{(h)}$ (“h” for observer “horizon”) where the worldlines of one of the families of test observers become null and the corresponding point of view is no longer valid. In the rotating Minkowski case the light cylinder exists only

Table 3. Causal restrictions, spatial gravitational force field quantities, and geodesic and null conditions for circular orbits in the Kerr spacetime.

	Kerr
length scale \mathcal{R}	\mathcal{M}
threading region of validity	$r > r_{(\text{erg})} = 2\mathcal{M}$
slicing region of validity	$r > r_{(\text{h})} = \mathcal{M} + \sqrt{\mathcal{M}^2 - a^2}$
$\nu(m, n)^{\hat{\phi}} = -\nu(n, m)^{\hat{\phi}}$	$-\frac{2a\mathcal{M}}{r\sqrt{\Delta}}$
gravitoelectric field	$g(m)^{\hat{r}} = -\frac{\mathcal{M}\sqrt{\Delta}}{r^2(r-2\mathcal{M})} < 0$ $g(n)^{\hat{r}} = -\frac{\mathcal{M}[(r^2+a^2)^2-4a^2\mathcal{M}r]}{r^2\sqrt{\Delta}(r^3+a^2r+2a^2\mathcal{M})} < 0$
gravitomagnetic field	$H(m)^{\hat{z}} = \frac{2a\mathcal{M}}{r^2(r-2\mathcal{M})} > 0$ $H(n, e_0)^{\hat{z}} = \frac{2a\mathcal{M}}{r^3} > 0$
expansion	$\theta(n)_{\hat{r}\hat{\phi}} = -\frac{a\mathcal{M}(3r^2+a^2)}{r^2(r^3+a^2r+2a^2\mathcal{M})} < 0$
signed relative curvature	$\kappa(\phi, m)^{\hat{r}} = -\frac{r(r-2\mathcal{M})^2 - \mathcal{M}a^2}{r^2\sqrt{\Delta}(r-2\mathcal{M})}$ $\kappa(\phi, n)^{\hat{r}} = -\frac{\sqrt{\Delta}(r^3-a^2\mathcal{M})}{r^2(r^3+a^2r+2a^2\mathcal{M})}$
counter-rotating and co-rotating timelike geodesics	$\dot{\phi}_{\pm} = \frac{\pm\sqrt{\mathcal{M}/r^3}}{1\pm a\sqrt{\mathcal{M}/r^3}}$ $\nu(U_{\pm}, m)^{\hat{\phi}} = \frac{\sqrt{\Delta}}{a_{\pm}(r-2\mathcal{M})\sqrt{r/\mathcal{M}}}$ $\nu(U_{\pm}, n)^{\hat{\phi}} = \frac{a^2 \mp 2a\sqrt{\mathcal{M}r+r^2}}{\sqrt{\Delta}(a_{\pm}r\sqrt{r/\mathcal{M}})}$
null orbits	$\zeta_{\pm} = \frac{2a\mathcal{M} \pm r\sqrt{\Delta}}{r^3+a^2r+2a^2\mathcal{M}}$

in the threading point of view and it occurs at the radius for which $|\nu(m, n)^{\hat{\phi}}| = 1$, while in the Gödel case it exists only in the slicing point of view where it occurs when $|\nu(n, m)^{\hat{\phi}}| = 1$. However, beyond that horizon $g_{\phi\phi}$ becomes negative, leading to the famous closed timelike ϕ coordinate lines. In the Kerr case where discussion is confined to the equatorial plane, the situation is reversed and the relative velocity is a decreasing function of r leading to an inner light radius. The slicing point of view is valid outside the event horizon which occurs at the value of r for which $\Delta = 0$, while the threading point of view is valid for $r > r_{(\text{erg})}$ outside the ergosphere (which in turn surrounds the event horizon), where $r_{(\text{erg})}$ is determined by the condition $|\nu(m, n)^{\hat{\phi}}| = 1$. The Gödel slicing observers attempt to resist the global rotation of the spacetime, but are forced to corotate at the outer observer horizon; similarly the threading and slicing observers in Kerr are forced to corotate at their respective inner observer horizons, namely the ergosphere and the event horizon.

The gravitoelectric field is the sign-reversed acceleration of the observer congruence, thus revealing the accelerations which characterize the threading and slicing observers. For example, in the rotating Minkowski spacetime the threading observers are accelerated radially inward while the counter-rotating slicing observers

(at rest in a global inertial frame) have zero acceleration. In the Gödel spacetime the situation is reversed and the threading observers are not accelerated while the counter-rotating slicing observers are accelerated radially outward. In both cases an outward acceleration must be added to resist the global rotation of spacetime (more precisely, of the nonlinear reference frame) by counter-rotating. The equatorial Kerr slicing and threading observers are both accelerated radially outward to oppose the attraction of the central mass, leading to inward gravitoelectric fields which allow circular orbits even in the nonrotating Schwarzschild limit. In the Kerr case the threading observers counter-rotate with respect to the slicing observers and one finds that their acceleration is larger than the acceleration of the slicing observers.

In each case considered here the gravitomagnetic fields are along the positive z -direction. In both the rotating Minkowski and Gödel spacetime this is due to the fact that the shift 1-forms are along the positive ϕ direction and their physical components along that direction are increasing functions of r , while in Kerr spacetime the same 1-form physical component is a decreasing function of r but its sign is reversed. Thus in each case the sign of the radial gravitomagnetic force component depends only on the sign of the relative velocity of the test particle along the angular direction, namely a positive (outward) force for co-rotating orbits and a negative (inward) force for counter-rotating orbits, where here the terms corotating and counter-rotating are with respect to the given observer family. Note also that in the Gödel spacetime the threading and slicing gravitomagnetic fields are the same and uniform (spatially covariant constant). That they are equal can also be seen directly from the transformation law for the gravitomagnetic vector field given in equation (11.6) of Ref. 5 and using the fact that the threading gravitoelectric field and the Lie derivative along e_0^α of the shift are zero and that the relative projection $P(m, n)^{-1}$ reduces to the identity along the radial direction orthogonal to the plane of the relative motion of the two observers. As discussed in [BCJ1], the expansion tensor, zero in the threading point of view, has one possibly nonvanishing r - ϕ component which is zero (rotating Minkowski) or negative (Gödel and Kerr) in the hypersurface and slicing points of view. Like the radial gravitomagnetic vector force, the radial expansion force is also positive (outward) for co-rotating orbits and negative (inward) for counter-rotating orbits, again with the sense of rotation referred here to the observer family. The sum of the gravitomagnetic vector force and the expansion force equals the total gravitomagnetic tensor force as discussed in [BCJ1].

On the other hand, the signed relative curvatures can change sign within the range of validity of one point of view yielding radial centripetal accelerations (sign-reversal of the space curvature forces) that can be either inward ($\kappa(\phi, u)^{\hat{r}} < 0$, the usual case) or outward ($\kappa(\phi, u)^{\hat{r}} > 0$). Figure 1 shows $\kappa(\phi, u)^{\hat{r}}$ for the various cases in the threading and hypersurface points of view. The local extrema of $g_{\phi\phi}$ and $\gamma_{\phi\phi}$ are the points where the relative Lie centripetal acceleration changes sign and the relative curvature of the spatial trajectory vanishes, yielding the Lie relatively

straight trajectories which are also spatial geodesics in each point of view.

In Figure 1 and successive figures, the Gödel and Kerr diagrams are divided into regions A, B, and C by thick vertical dashed lines according to whether 2, 1, or 0 of the two oppositely directed circular geodesics are timelike. The boundaries of these regions, as discussed in detail in section 4, occur at the radii of the two null circular geodesics. Thin vertical dashed lines also mark the horizon and outer ergosphere radii in the Kerr case.

The behavior of the Lie relative curvature depends on the intrinsic geometry of the Riemannian metric on the quotient space appropriate to each point of view. In the threading case this metric is just the natural projection of the spatial metric to the observer-quotient space, while in the slicing point of view, it is instead the pullback of the spatial metric to the quotient by the threading congruence. For the case of planar orbits, 2-dimensional embedding diagrams in either 3-dimensional Euclidean space E_3 or 3-dimensional Minkowski spacetime M_3 as appropriate are useful to interpret the effects of this spatial geometry on the orbits in this plane, as well as on the precession of the spin of a gyroscope following such an orbit. Thorne⁵¹ has given an neat illustration of this latter effect in terms of the conical defect of the tangent cone in the embedding space. The details of the embedding are explained in the appendix, together with the actual diagrams of the cross-sectional curves of these surfaces of revolution.

3. Circular geodesics

The timelike circular geodesics are the circular orbits along which the relative spatial force $F(U, u)^{\hat{r}}$ vanishes. The relative velocities corresponding to these geodesics can then be found by setting to zero the sum of the Lie spatial gravitational force and the space curvature force, leading to a quadratic equation in those velocities or in the coordinate angular velocities (linear when $\kappa(\phi, u)^{\hat{r}} = 0$). The regions where the geodesics are timelike are those regions where the corresponding spatial relative speeds are smaller than 1 (provided that the observers are also timelike). Let U_{\pm}^{α} , $\nu(U_{\pm}, u)^{\alpha}$, and $\dot{\phi}_{\pm}$ be the 4-velocity, relative velocity, and coordinate angular velocity of the corotating (+) and counter-rotating (−) geodesics in each spacetime, when they exist.

For example, in the rotating Minkowski case there are only counter-rotating circular geodesics, which correspond to the points fixed in the global inertial frame with respect to which the rotating nonlinear reference frame rotates, namely the orbits of the slicing observers ($\nu(U_{-}, n)^{\hat{\phi}} = 0$ in Tables 2 and 3. These worldlines are clearly timelike everywhere. Their spatial velocity relative to the threading observers becomes larger than the velocity of light when $\Omega r > 1$ only because the threading observer congruence becomes spacelike there. In the Gödel spacetime the co-rotating geodesics are instead the orbits of the threading observers ($\nu(U_{+}, m)^{\hat{\phi}} = 0$). These worldlines are then timelike in the region of validity of the threading point of view, i.e., everywhere. On the other hand the counter-rotating geodesics are timelike as long as $|\nu(U_{-}, m)^{\hat{\phi}}| < 1$ or $|\nu(U_{-}, n)^{\hat{\phi}}| < 1$ which gives $r < \frac{1}{2}r_{(h)}$. In

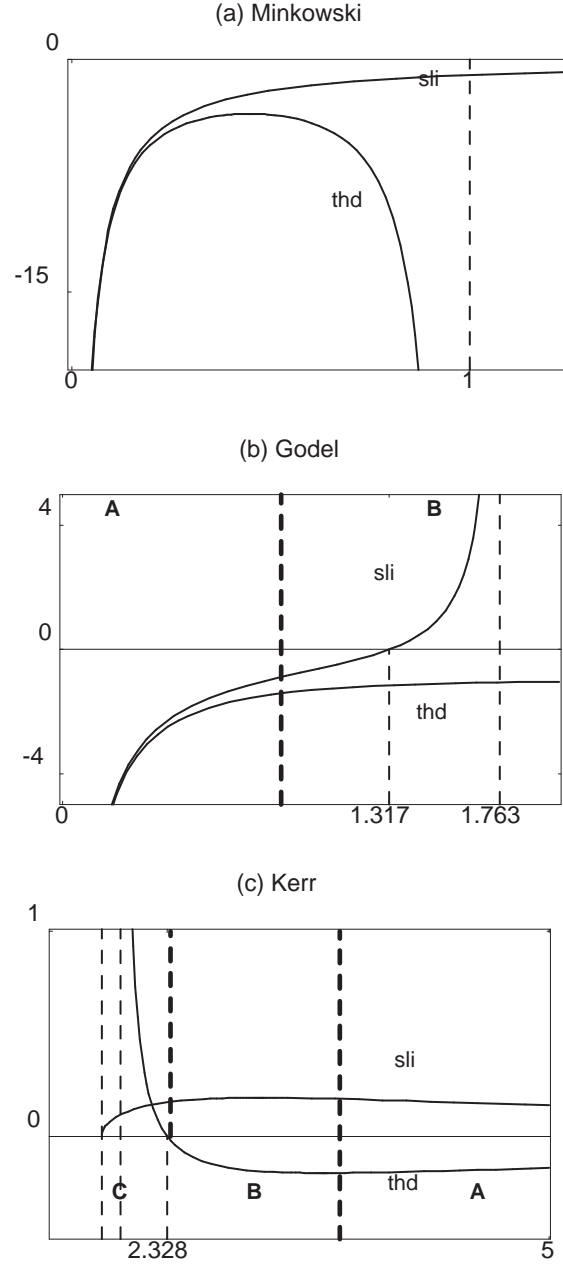


Fig. 1. κ versus \bar{r} : plots of the signed Lie relative curvature $\kappa(\phi, u)^{\bar{r}}$ of the circular orbits in the equatorial plane of the rotating Minkowski, Gödel, and $a/M = 1/2$ Kerr spacetimes in the threading ($u = m$) and hypersurface ($u = n$) points of view as functions of $\bar{r} = r/\mathcal{R}$ (Minkowski, Gödel) or $\bar{r} = r/M$ (Kerr). In this particular Kerr case the relatively straight circle occurs just inside the region C (which begins at $\bar{r} \approx 2.35$) described below.

the Kerr spacetime the equations $|\nu(U_{\mp}, n)^{\hat{\phi}}| = 1$ and $|\nu(U_{\mp}, m)^{\hat{\phi}}| = 1$ have roots (valid only within the region of validity of each point of view) at $r(r - 3\mathcal{M}) = \pm 2a\mathcal{M}\sqrt{r/\mathcal{M}}$. In the extreme Kerr case $a = \mathcal{M}$, these roots are $r = \mathcal{M}$ for the co-rotating geodesics and $r = 4\mathcal{M}$ for the counter-rotating geodesics.

Tables 2 and 3 show that for the Gödel and Kerr spacetimes which have two oppositely directed circular geodesics, both the magnitude of the coordinate angular velocity ζ and of the angular component of the velocity $\nu(U, u)^{\hat{\phi}}$ are larger for geodesics in the counter-rotating direction than in the corotating direction in both the threading and slicing points of view. This immediately implies that the geodesic gamma factor $\gamma(U_{\pm}, u)$ and with some additional reasoning the coordinate gamma factor $\Gamma(U_{\pm}, u)$ are also both larger in the counter-rotating direction than in the corotating direction. The latter follows from the former using the slicing representation of the coordinate gamma factor given in Eq. (2.10). This general counter-rotation effect manifested in this asymmetry between the co-rotating and counter-rotating directions is the direct consequence of an upward gravitomagnetic field which adds an inward radial force to the total sum for the counter-rotating case increasing the speed, and an outward radial force to the total sum for the corotating case decreasing the speed.

The asymmetry in the coordinate angular velocity between the corotating and the counter-rotating circular geodesics is the origin of the precession of their alternating meeting points (after a full revolution, not half a revolution) in the counter-rotating direction. Analogous to the zero Sagnac effect (slicing) observers which follow Killing trajectories containing the meeting points of oppositely directed circular null paths, one can introduce “geodesic meeting point observers” (only in the equatorial plane in Kerr⁸) containing the meeting points of the oppositely directed circular geodesics. Their angular velocity is analogously the average (see Tables 2 and 3)

$$\zeta_{(\text{gmp})} = (\dot{\phi}_{-} + \dot{\phi}_{+})/2 . \quad (3.1)$$

For Kerr this has the negative value $\zeta_{(\text{gmp})} = -a\mathcal{M}r^{-3}/(1 - a^2\mathcal{M}r^{-3})$, and for Gödel it is also negative $\zeta_{(\text{gmp})} = \dot{\phi}_{-}/2$ since $\dot{\phi}_{+} = 0$. Using Eqs (2.8), (2.9), one can show that the slicing velocities are also related by averaging

$$\nu(U_{(\text{gmp})}, n)^{\hat{\phi}} = [\nu(U_{-}, n)^{\hat{\phi}} + \nu(U_{+}, n)^{\hat{\phi}}]/2 , \quad (3.2)$$

as is trivially the case for the slicing velocities of the null meeting point observers and the oppositely directed null paths.

The spatial equation of motion evaluated along the circular geodesics with zero total spatial force describes how the various radial spatial forces balance. In the threading point of view the expansion is zero because of the stationary symmetry so only the gravitoelectric, the vector gravitomagnetic, and the space curvature forces are present. In the hypersurface point of view the gravitomagnetic field vanishes and one is left with only the vector gravitoelectric, expansion, and space curvature forces. In the slicing point of view all the forces contribute to the radial force balance equation. Figures 2 and 3 show the plots of the various radial forces (divided by

the common factor $\gamma(U, u)$ evaluated along the circular geodesics as functions of the radial coordinate r in the several points of view and for the various cases. To better visualize the results, some suggestive 3-dimensional diagrams showing the balance of the various forces in space may be found in Carini, Bini and Jantzen,⁹ with relative magnitudes of the various forces given in the limit of small rotational speeds, i.e., near the axis of symmetry in the rotating Minkowski and Gödel cases, and far from the black hole in the Kerr case. We now discuss the force balance for each of the three spacetimes under consideration.

3.1. Rotating Minkowski spacetime

In the rotating Minkowski spacetime the radial force equation reduces respectively in the threading, hypersurface, and slicing points of view to

$$\begin{aligned}
-F(U, m)^{\hat{r}} &= F^{(\text{SC})}(U, m)^{\hat{r}} + F^{(\text{GM})}(U, m)^{\hat{r}} + F^{(\text{GE})}(U, m)^{\hat{r}} \\
&= \gamma(U, m) \left\{ \left[\gamma^2 \frac{|\nu(U, m)^{\hat{\phi}}|^2}{r} \right] + \left[2\gamma^2 \nu(U, m)^{\hat{\phi}} \Omega \right] + \left[\gamma^2 \Omega^2 r \right] \right\} \\
&= \gamma(U, m) \frac{\gamma^2}{r} (\nu(U, m)^{\hat{\phi}} + \Omega r)^2, \\
-F(U, n)^{\hat{r}} &= F^{(\text{SC})}(U, n)^{\hat{r}} = \gamma(U, n) \frac{|\nu(U, n)^{\hat{\phi}}|^2}{r}, \\
-F(U, n, e_0)^{\hat{r}} &= F^{(\text{SC})}(U, n, e_0)^{\hat{r}} + F^{(\text{GM})}(U, n, e_0)^{\hat{r}} \\
&= \gamma(U, n) \left\{ \left[\frac{|\nu(U, n)^{\hat{\phi}}|^2}{r} - \Omega \nu(U, n)^{\hat{\phi}} \right] + \left[\Omega \nu(U, n)^{\hat{\phi}} \right] \right\}. \quad (3.3)
\end{aligned}$$

Table 4 shows the explicit expressions of the various spatial forces evaluated along the circular geodesics where they balance.

Table 4. The various spatial radial forces divided by a common factor $\gamma(U, u)$ evaluated along the equatorial counter-rotating circular geodesics are given as functions of r in the various points of view.

Rotating Minkowski Spacetime				
	$\gamma^{-1} F^{(\text{SC})\hat{r}}$	$\gamma^{-1} F^{(\text{GM})\hat{r}}$	$\gamma^{-1} F^{(\text{EX})\hat{r}}$	$\gamma^{-1} F^{(\text{GE})\hat{r}}$
Thd ₋	$\gamma^2 \Omega^2 r$	$-2\gamma^2 \Omega^2 r$	0	$\gamma^2 \Omega^2 r$
Hyp ₋	0	0	0	0
Sli ₋	0	0	0	0

The geodesics are the orbits of particles at rest in the associated global inertial frame with respect to which the rotation takes place. In the threading point of view these orbits must counter-rotate in order to compensate for the rotation of the threading observers and the outward gravitoelectric force and space curvature force along them are equal and add together to balance the inward gravitomagnetic force. On the other hand the slicing observers are simply the fixed observers in the

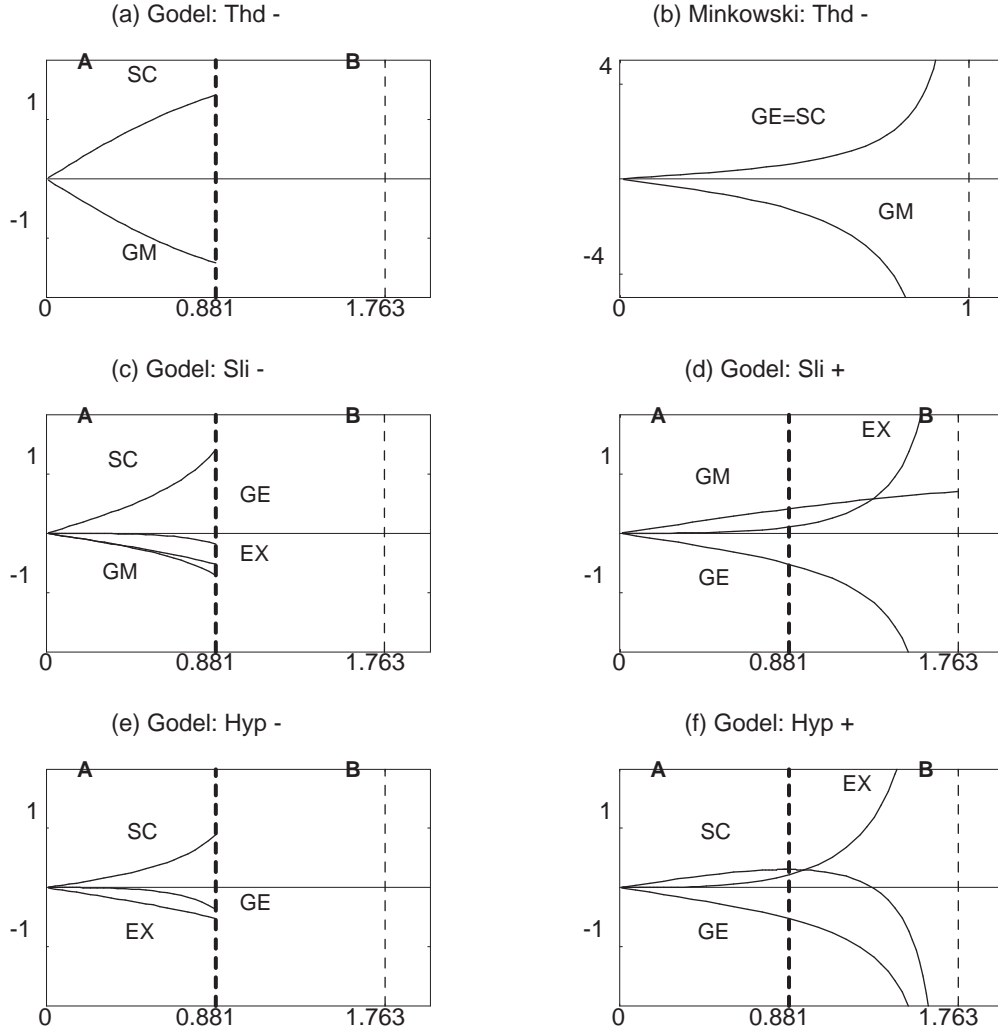


Fig. 2. F versus \bar{r} : plots of the space curvature (SC), gravitomagnetic (GM), expansion (EX), and gravitoelectric (GE) spatial radial forces (divided by a common $\gamma(U, u)$ factor and multiplied by \mathcal{R}) along the corotating (+) and counter-rotating (-) circular geodesics in the rotating Minkowski and Gödel spacetimes in the threading (thd), hypersurface (hyp) and slicing (sli) points of view, plotted versus the rescaled radial coordinate \bar{r} . The horizontal ranges for the Gödel counter-rotating/corotating cases are respectively $r \in [0, r_{(h)}/2]$ and $r \in [0, r_{(h)}]$. The thick dashed vertical line separates the region A near the origin where both circular geodesics are timelike from the region B where only the corotating geodesic is timelike. The observer horizons are marked by a thin dashed vertical line.

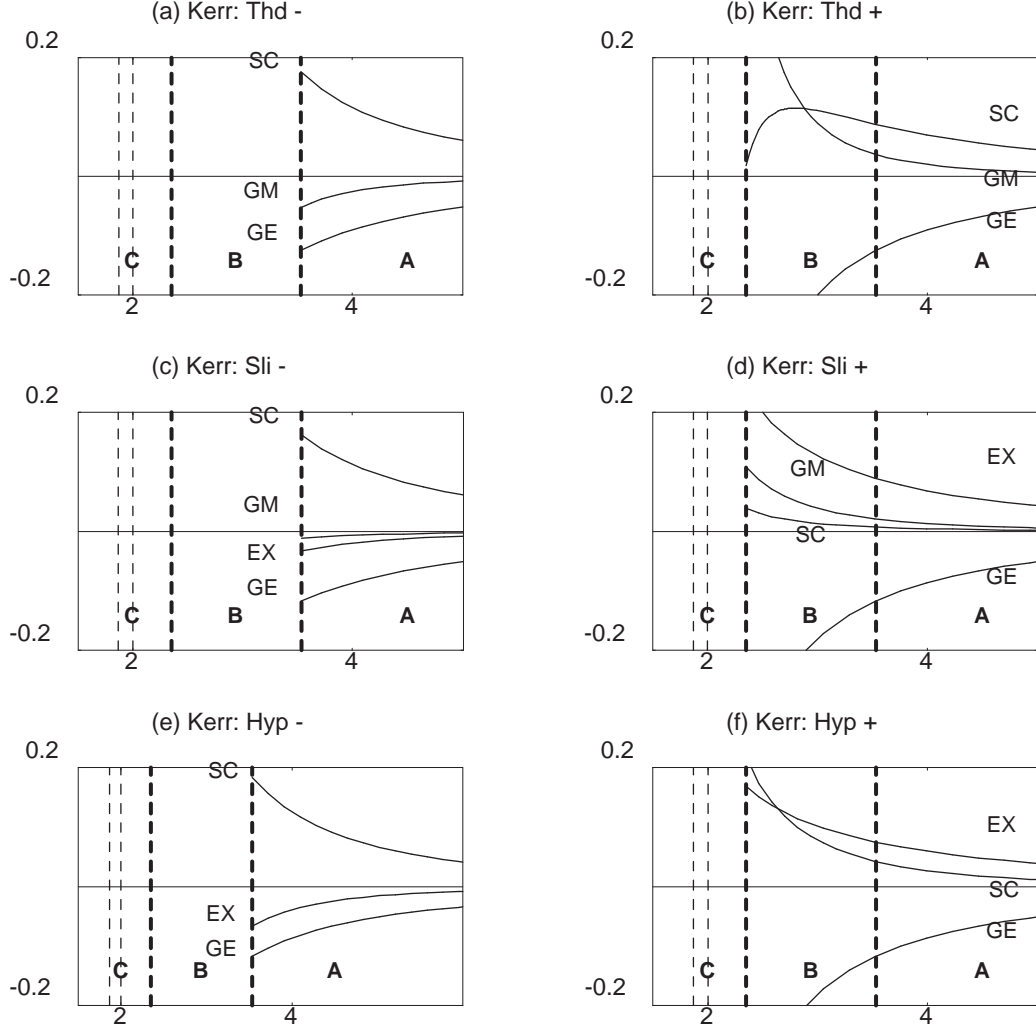


Fig. 3. F versus \bar{r} : plots of the space curvature (SC), gravitomagnetic (GM), expansion (EX) and gravitoelectric (GE) spatial radial forces (multiplied by $\mathcal{M}/\gamma(U, u)$) along the corotating (+) and counter-rotating (-) equatorial circular geodesics around a Kerr black hole with $a/M = 0.5$, in the threading (thd), hypersurface (hyp), and slicing (sli) points of view as a function of $\bar{r} = r/M$. The thick dashed vertical lines at $\bar{r} \approx 2.35, 3.53$ separate the three regions A which extends out to infinity, C which extends inward to the horizon ($\bar{r}_{\text{hor}} \approx 1.87$) and B which is sandwiched in between them and which contains the ergosphere boundary ($\bar{r}_{\text{erg}} = 2$). The observer horizons are marked by thin dashed vertical lines.

nonrotating Minkowski spacetime and so they experience no spatial gravitational field in the hypersurface point of view. However, in cylindrical coordinates they measure a radially outward space curvature force, which vanishes only along the circular geodesics and it is due to the curvature of the circular ϕ coordinates rather than to a real curvature of the space which is actually flat.

In the slicing point of view there is a gravitomagnetic force and a space curvature force but again both vanish along the circular geodesics. The relation between the threading and the hypersurface points of view in this case is given simply by the addition of velocity formula

$$\begin{aligned}\nu(U, n)^{\hat{\phi}} &= \frac{\nu(U, m)^{\hat{\phi}} + \Omega r}{1 + \nu(U, m)^{\hat{\phi}} \Omega r}, \\ \gamma(U, n) &= \gamma \gamma(U, m) (1 + \nu(U, m)^{\hat{\phi}} \Omega r),\end{aligned}\quad (3.4)$$

which just shows that the two points of view are related by a boost.

3.2. Gödel spacetime

The radial force equations for the circular orbits in the Gödel spacetime in the threading, hypersurface, and slicing points of view respectively are

$$\begin{aligned}-F(U, m)^{\hat{r}} &= F^{(\text{SC})}(U, m)^{\hat{r}} + F^{(\text{GM})}(U, m)^{\hat{r}} \\ &= \gamma(U, m) \left\{ \left[\sqrt{2} \Omega T^{-1} |\nu(U, m)^{\hat{\phi}}|^2 \right] + \left[2 \Omega \nu(U, m)^{\hat{\phi}} \right] \right\}, \\ -F(U, n)^{\hat{r}} &= F^{(\text{SC})}(U, n)^{\hat{r}} + F^{(\text{EX})}(U, n)^{\hat{r}} + F^{(\text{GE})}(U, n)^{\hat{r}} \\ &= \gamma(U, n) \left\{ \left[\frac{\sqrt{2} \Omega (1 - 2s^2)}{2t(1 - s^2)} |\nu(U, n)^{\hat{\phi}}|^2 \right] \right. \\ &\quad \left. + \left[\frac{2\Omega s^2}{1 - s^2} \nu(U, n)^{\hat{\phi}} \right] - \left[\frac{\sqrt{2} \Omega t}{1 - s^2} \right] \right\}, \\ -F(U, n)^{\hat{r}} &= F^{(\text{SC})}(U, n, e_0)^{\hat{r}} + F^{(\text{GM})}(U, n, e_0)^{\hat{r}} + F^{(\text{EX})}(U, n, e_0)^{\hat{r}} \\ &\quad + F^{(\text{GE})}(U, n)^{\hat{r}} \\ &= \gamma(U, n) \left\{ \left[\frac{\sqrt{2} \Omega (1 - 2s^2)}{2t(1 - s^2)} |\nu(U, n)^{\hat{\phi}}|^2 - \frac{\Omega (1 - 2s^2)}{1 - s^2} \nu(U, n)^{\hat{\phi}} \right] \right. \\ &\quad \left. + \left[\Omega \nu(U, n)^{\hat{\phi}} \right] + \left[\frac{\Omega s^2}{1 - s^2} \nu(U, n)^{\hat{\phi}} \right] - \left[\frac{\sqrt{2} \Omega t}{1 - s^2} \right] \right\}.\end{aligned}\quad (3.5)$$

Table 5 shows the values of the various spatial forces evaluated along the two sets of geodesics where the forces balance.

In this case the threading observers move along (corotating) geodesics which are the same trajectories as the dust particles, while a second family of geodesics counter-rotates as in the rotating Minkowski case. In the threading point of view the outward space curvature force balances the inward gravitomagnetic force along these counter-rotating geodesics, while all forces vanish for the corotating geodesics.

Table 5. The various spatial radial forces divided by a common factor $\gamma(U, u)$ evaluated along the counter-rotating (subscript $-$) and corotating (subscript $+$) circular geodesics are given as functions of r in various points of view.

Gödel spacetime				
	$\gamma^{-1} F^{(\text{SC})\hat{r}}$	$\gamma^{-1} F^{(\text{GM})\hat{r}}$	$\gamma^{-1} F^{(\text{EX})\hat{r}}$	$\gamma^{-1} F^{(\text{GE})\hat{r}}$
Thd $_-$	$2\sqrt{2}\Omega T$	$-2\sqrt{2}\Omega T$	0	0
Hyp $_-$	$\frac{\sqrt{2}\Omega t}{(1-s^2)(1-2s^2)}$	0	$-\frac{2\sqrt{2}\Omega ts^2}{(1-s^2)(1-2s^2)}$	$-\frac{\sqrt{2}\Omega t}{1-s^2}$
Sli $_-$	$\frac{2\sqrt{2}\Omega t}{1-2s^2}$	$-\frac{\sqrt{2}\Omega t}{1-2s^2}$	$-\frac{\sqrt{2}\Omega ts^2}{(1-s^2)(1-2s^2)}$	$-\frac{\sqrt{2}\Omega t}{1-s^2}$
Thd $_+$	0	0	0	0
Hyp $_+$	$\frac{\sqrt{2}\Omega t(1-2s^2)}{1-s^2}$	0	$\frac{2\sqrt{2}\Omega ts^2}{1-s^2}$	$-\frac{\sqrt{2}\Omega t}{1-s^2}$
Sli $_+$	0	$\sqrt{2}\Omega t$	$\frac{\sqrt{2}\Omega ts^2}{1-s^2}$	$-\frac{\sqrt{2}\Omega t}{1-s^2}$

In the slicing point of view, the space curvature force for the corotating geodesics vanishes due to the factor $[\nu(U, n)^\phi - N^{-1}N^\phi]\nu(U, n)^\phi = N^{-1}\dot{\phi}\nu(U, n)^\phi$ in equation (2.15) which vanishes for $\dot{\phi} = 0$. Both the hypersurface and slicing space curvature forces for the counter-rotating geodesics and the hypersurface space curvature force become negative, corresponding to a Lie centripetal acceleration directed radially outward, for $r > r_{(\text{rs})} > r_{(\text{h})}/2$, where $\bar{r}_{(\text{rs})} = 2\text{arcsinh}(2^{-1/2}) \approx 1.317$ defines the Lie relatively straight trajectory. This effect is closely related to the result discussed at length by Abramowicz et al in the case of circular orbits in the Schwarzschild spacetime and just corresponds to the turning back of the embedded 2-surface of revolution towards its axis as shown in the appendix. However, the counter-rotating geodesic is only timelike for $r < r_{(\text{h})}/2$.

3.3. *Kerr spacetime*

Here one finds the following spatial forces respectively in the threading, hypersurface, and slicing points of view

$$\begin{aligned}
-F(U, m)^{\hat{r}} &= F^{(\text{SC})}(U, m)^{\hat{r}} + F^{(\text{GM})}(U, m)^{\hat{r}} + F^{(\text{GE})}(U, m)^{\hat{r}} \\
&= \gamma(U, m) \left\{ \left[\frac{r(r-2\mathcal{M})^2 - \mathcal{M}a^2}{r^2\sqrt{\Delta}(r-2\mathcal{M})} |\nu(U, m)^{\hat{\phi}}|^2 \right] \right. \\
&\quad \left. + \left[\frac{2a\mathcal{M}}{r^2(r-2\mathcal{M})} \nu(U, m)^{\hat{\phi}} \right] - \left[\frac{\mathcal{M}\sqrt{\Delta}}{r^2(r-2\mathcal{M})} \right] \right\}, \\
-F(U, n)^{\hat{r}} &= F^{(\text{SC})}(U, n)^{\hat{r}} + F^{(\text{EX})}(U, n)^{\hat{r}} + F^{(\text{GE})}(U, n)^{\hat{r}} \\
&= \gamma(U, n) \left\{ \left[\frac{\sqrt{\Delta}(r^3 - a^2\mathcal{M})}{r^2(r^3 + a^2r + 2a^2\mathcal{M})} |\nu(U, n)^{\hat{\phi}}|^2 \right] \right. \\
&\quad \left. + \left[\frac{2a\mathcal{M}(3r^2 + a^2)}{r^2(r^3 + a^2r + 2a^2\mathcal{M})} \nu(U, n)^{\hat{\phi}} \right] \right\}
\end{aligned}$$

$$\begin{aligned}
 -F(U, n)^{\hat{r}} &= F^{(\text{SC})}(U, n, e_0)^{\hat{r}} + F^{(\text{GM})}(U, n, e_0)^{\hat{r}} + F^{(\text{EX})}(U, n, e_0)^{\hat{r}} \\
 &\quad + F^{(\text{GE})}(U, n)^{\hat{r}} \\
 &= \gamma(U, n) \left\{ \left[\frac{\mathcal{M}[(r^2 + a^2)^2 - 4a^2\mathcal{M}r]}{r^2\sqrt{\Delta}(r^3 + a^2r + 2a^2\mathcal{M})} \right] \right. \\
 &\quad \left. - \frac{\sqrt{\Delta}(r^3 - a^2\mathcal{M})}{r^2(r^3 + a^2r + 2a^2\mathcal{M})} |\nu(U, n)^{\hat{\phi}}|^2 \right. \\
 &\quad \left. - \frac{2a\mathcal{M}(a^2\mathcal{M} - r^3)}{r^3(r^3 + a^2r + 2a^2\mathcal{M})} \nu(U, n)^{\hat{\phi}} \right] \\
 &\quad + \left[\frac{a\mathcal{M}}{r^3} \nu(U, n)^{\hat{\phi}} \right] + \left[\frac{a\mathcal{M}(3r^2 + a^2)}{r^2(r^3 + a^2r + 2a^2\mathcal{M})} \nu(U, n)^{\hat{\phi}} \right] \\
 &\quad \left. - \left[\frac{\mathcal{M}[(r^2 + a^2)^2 - 4a^2\mathcal{M}r]}{r^2\sqrt{\Delta}(r^3 + a^2r + 2a^2\mathcal{M})} \right] \right\}. \tag{3.6}
 \end{aligned}$$

In both the threading and slicing points of view the addition of an upward (+ z direction) gravitomagnetic field, in comparison with the corresponding Schwarzschild case, adds a radially inward gravitomagnetic force for the counter-rotating circular geodesics and a radially outward one for the corotating geodesics. The coordinate angular velocity $\dot{\phi}_-$ of the counter-rotating geodesics thus increases in magnitude with respect to the Schwarzschild case while the coordinate angular velocity $\dot{\phi}_+$ of the corotating geodesics decreases in magnitude.

In the threading point of view, the space curvature force changes sign at the single real root $r_{(\text{rs})}$ of the equation $r(r - 2\mathcal{M})^2 - \mathcal{M}a^2 = 0$ which occurs outside the ergosphere in regions C and B, as shown in Figure 4, thus only affecting the corotating geodesics in region B. This corresponds to a Lie relatively straight trajectory which in the extreme case $\bar{a} = 1$ occurs at $\bar{r}_{(\text{rs})} = (3 + \sqrt{5})/2 \approx 2.618$, while for the example $\bar{a} = 0.5$ one has $\bar{r}_{(\text{rs})} \approx 2.328$. Note that the Lie centripetal acceleration points radially outward for $r < r_{(\text{rs})}$ while in Gödel it points outward for $r > r_{(\text{rs})}$, i.e., approaching the observer horizon in both cases.

4. Accelerated circular orbits

The physical non-gravitational force acting on a test particle that moves with 4-velocity U is just the 4-force $f(U)^\alpha$ which is related to the rescaled apparent 3-force by the equation (9.9) of [BCJ1], namely

$$F(U, u)^\alpha = \gamma(U, u)^{-1} P(u)^\alpha{}_\beta f(U)^\beta. \tag{4.1}$$

In the purely transverse relative acceleration applications that are considered here, the 4-force is along the radial direction where the projection reduces to the identity. The equation of motion may then be simply expressed in terms of the physical force by equation (14.7) of [BCJ1], namely

$$f(U)^{\hat{r}} = \gamma(U, u) F(U, u)^{\hat{r}} = \gamma(U, u) [-F^{(\text{SC})}(U, u)^{\hat{r}} - F_{(\text{lie})}^{(\text{G})}(U, u)^{\hat{r}}] = a(U)^{\hat{r}}. \tag{4.2}$$

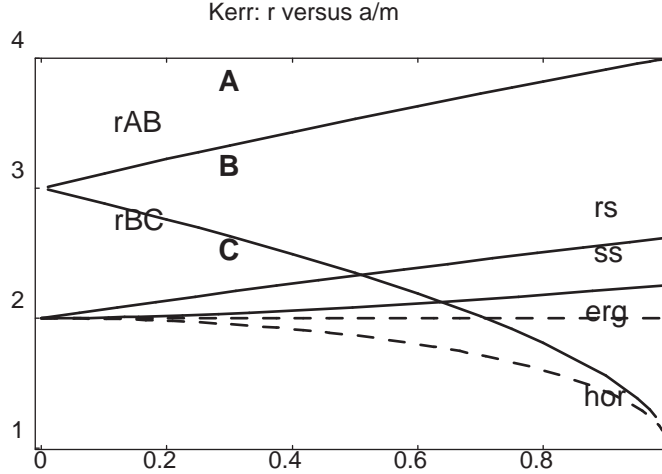


Fig. 4. \bar{r} versus \bar{a} : a plot of the Kerr Boyer-Lindquist radial coordinate \bar{r} versus $\bar{a} = a/M \in [0, 1]$ for the horizon (hor), outer ergosphere boundary (erg), the two boundaries between the regions A, B, and C, and the threading relatively straight circles (rs) and embedding signature-switching circles (ss) for the equatorial plane.

The middle equality is just the first of equations (2.13). This relationship enables one to express the single observer-independent quantity in terms of all the various points of view using equations (2.14) and (2.15). However, it is important to remember that for relative motion not of this kind, the situation is much more complicated.

In the present case the expression for the physical force (namely, the 4-acceleration by the equation of motion) is a quadratic expression in the relative velocity physical component $\nu(U, u)^{\hat{\phi}}$ multiplied by the square of the associated gamma factor, leading to a quotient of two quadratic expressions multiplied by a space curvature factor. The zeros of the denominator occur when the velocity approaches ± 1 , i.e., corresponding to photon orbits, values which bound the domain $(-1, 1)$ of allowed values of the velocity. The zeros of the numerator are just the velocities which correspond to circular geodesic motion and may occur inside (subluminal) or outside (superluminal) the physical domain $(-1, 1)$ of the function of the velocity.

As noticed by Barrabes, Boisseau and Israel³⁴ in their discussion of the hypersurface point of view for Kerr and Schwarzschild, it is very useful to express the numerator of the physical radial force expression in the explicitly factorized form

$$\begin{aligned} f(U)^{\hat{r}} &= \kappa(\phi, u)^{\hat{r}} \gamma(U, u)^2 [\nu(U, u)^{\hat{\phi}} - \nu(U_-, u)^{\hat{\phi}}] [\nu(U, u)^{\hat{\phi}} - \nu(U_+, u)^{\hat{\phi}}] \\ &= -\kappa(\phi, n)^{\hat{r}} \frac{(\zeta - \dot{\phi}_-)(\zeta - \dot{\phi}_+)}{(\zeta - \zeta_-)(\zeta - \zeta_+)} \end{aligned} \quad (4.3)$$

valid when $\kappa(\phi, u)^{\hat{r}} \neq 0$, where the roots of these factors in the first case are the geodesic velocities ($\nu(U_-, u)^{\hat{\phi}} \leq \nu(U_+, u)^{\hat{\phi}}$), at least one of which blows up when $\kappa(\phi, u)^{\hat{r}} = 0$ so that the force remains finite when other terms besides the centripetal

acceleration term are present. This also applies to the Minkowski spacetime with $\nu(U_-, u)^{\hat{\phi}} = \nu(U_+, u)^{\hat{\phi}}$. Although the right hand side of this equation contains observer-dependent quantities, the expression itself is observer-independent since it represents the physical force acting on the test particle. Thus in general, even when the spatial curvature force changes sign due to a change in sign of $\kappa(\phi, u)^{\hat{r}}$, the total force will not. The analogous expression for the zero rest mass particle is

$$\begin{aligned} f(P_{\pm})^{\hat{r}} &= \kappa(\phi, u)^{\hat{r}} E(P_{\pm}, u)^2 [\pm 1 - \nu(U_-, u)^{\hat{\phi}}] [\pm 1 - \nu(U_+, u)^{\hat{\phi}}] \\ &= 4E(P_{\pm}, n)^2 \kappa(\phi, n)^{\hat{r}} (\zeta_{\pm} - \dot{\phi}_{\pm}) (\zeta_{\pm} - \dot{\phi}_{\pm}) / (\zeta_{-} - \zeta_{+})^2 . \end{aligned} \quad (4.4)$$

de Felice^{27, 28} first used such a factorization (4.3) of the physical radial force for Kerr expressed in terms of the coordinate angular velocities rather than the physical component of the relative velocities along the orbit. The new angular velocity parameter $y = \zeta / (1 - a\zeta)$ (a fractional linear transformation) he uses in place of the parameter ζ (his Ω) of equation (2.2) for constant angular velocity world lines corresponds locally but not globally to a new choice of slicing by a local time function $t' = t - a\phi$ as discussed in the appendix of Greene, Schucking, and Vishveshwara.⁴³ Although a global such function does not exist, one can introduce it as a well-defined change of parametrization on the world lines of test particles. The advantage of this is that the new expressions for the coordinate angular velocity $d\phi/dt'$ of timelike circular geodesics in the equatorial plane of Kerr are reduced to the simpler Schwarzschild form, while retaining the feature that the physical force is still a quotient of quadratic expressions in this new parameter, as in the case of the original angular velocity parameter ζ and also for the physical component of the relative velocity in each point of view. Note that the physical force is a fractional quadratic function of the relative velocity, as it is also of any new variable differing from the relative velocity by a fractional linear transformation, like ζ or y , or the change in relative velocity from changing the observer.

Comparing the full expression for the physical force expressed in terms of the relative acceleration, gravitoelectric, and gravitomagnetic terms in the threading point of view

$$f(U)^{\hat{r}} = \gamma(U, m)^2 [\kappa(\phi, m)^{\hat{r}} \nu(U, m)^{\hat{\phi}2} - \nu(U, m)^{\hat{\phi}} H(m)^{\hat{z}} - g(m)^{\hat{r}}] \quad (4.5)$$

leads to the identification

$$\begin{aligned} g(m)^{\hat{r}} &= -\kappa(\phi, m)^{\hat{r}} \nu(U_-, m)^{\hat{\phi}} \nu(U_+, m)^{\hat{\phi}} , \\ H(m)^{\hat{z}} &= \kappa(\phi, m)^{\hat{r}} [\nu(U_-, m)^{\hat{\phi}} + \nu(U_+, m)^{\hat{\phi}}] . \end{aligned} \quad (4.6)$$

Similar relations hold for the hypersurface point of view with $H(m)^{\hat{z}}$ replaced by $-2\theta(n)_{r\phi} = H(n, e_0)^{\hat{z}} + 2\kappa(\phi, n)^{\hat{r}} \nu(e_0, n)^{\hat{\phi}}$. In the usual case in which the signed Lie curvature is negative, an upward gravitomagnetic vector field corresponds to a negative sum for the two geodesic velocities, as will be assumed in discussion below unless explicitly specified.

Consider the case of a circular orbit for which the Lie signed relative curvature $\kappa(\phi, u)^{\hat{r}} < 0$, i.e., the familiar case in which the appropriate derivative of the Lie relative tangent vector is inward along the radial direction. Then the physical force is positive (outward) if $\nu(U_-, u)^{\hat{\phi}} < \nu(U, u)^{\hat{\phi}} < \nu(U_+, u)^{\hat{\phi}}$ and it is negative (inward) if $\nu(U, u)^{\hat{\phi}} > \nu(U_+, u)^{\hat{\phi}}$ or $\nu(U, u)^{\hat{\phi}} < \nu(U_-, u)^{\hat{\phi}}$. This result is exactly what one would expect in Newtonian gravity: namely, an outward push is necessary to remain on a circular orbit if the speed is less than the geodesic speed (Keplerian speed in the Newtonian context), while an inward push is necessary if the speed is larger than the geodesic speed.

However, again as in Newtonian gravity, if the speed is larger than the geodesic speed and one increases it, the inward force necessary to maintain the circular orbit must also increase in magnitude and vice versa. This is not always true in the general relativistic case, not only in strong gravitational fields but also in certain weak gravitational fields. To investigate this property, one needs not only the sign of $f(U)^{\hat{r}}$ but also the sign of its derivative with respect to the velocity of the test particle $\nu(U, u)^{\hat{\phi}}$ for a given point of view.

This analysis is governed by the 3-parameter family of functions

$$\mathcal{F}(\nu; \kappa, \nu_-, \nu_+) = \kappa[\nu - \nu_-][\nu - \nu_+]/[1 - \nu^2] \quad (4.7)$$

of the real variable ν and by its derivative with respect to that variable. A specific spacetime and choice of observers collapses this family of functions to a 1-parameter family in which κ, ν_-, ν_+ all depend on the radial coordinate. The way in which this collapse takes place leads to many possible behaviors. One must also be careful taking limits of this expression in which ν and another velocity parameter go to ± 1 , since the order in which the limits are taken matters.

The qualitative behavior of family of force versus velocity graphs (for different radii) is characterized first by the number of distinct real roots of the force function for a given radius, and second by the number of such roots which lie in the physical interval $(-1, 1)$ of “subluminal” values for nonzero rest mass test particle motion. One can distinguish three different regions of the spacetime (which may or may not be present) containing those radii for which one of the following conditions holds (assuming $\nu_- + \nu_+ \leq 0$)

region A: ν_-, ν_+ both subluminal,

region B: ν_+ subluminal, ν_- superluminal,

region C: ν_-, ν_+ both superluminal.

When they exist, the interfaces between regions A and B and regions B and C are at the radii $r_{(AB)}$ and $r_{(BC)}$ at which the circular null geodesics occur.

Within each of these three regions, the qualitative properties of the force function are similar and follow from the expressions for its first and second derivatives

$$d\mathcal{F}(\nu; \kappa, \nu_-, \nu_+)/d\nu$$

$$\begin{aligned}
 &= -\kappa[(\nu_- + \nu_+)(\nu^2 + 1) - 2\nu(1 + \nu_- \nu_+)]/[1 - \nu^2]^2 \\
 &= -\kappa(\nu_- + \nu_+)[\nu^2 - 2\nu/\nu_{(\text{rel})} + 1]/[1 - \nu^2]^2 \\
 &= -\kappa(\nu_- + \nu_+)[\nu - \nu_{(\text{crit})-}][\nu - \nu_{(\text{crit})+}]/[1 - \nu^2]^2 , \\
 d^2 \mathcal{F}(\nu; \kappa, \nu_-, \nu_+)/d\nu^2 \\
 &= -2\kappa[(\nu_- + \nu_+)(\nu^2 + 3)\nu - (3\nu^2 + 1)(1 + \nu_- \nu_+)]/[1 - \nu^2]^3 \\
 &= -2\kappa(\nu_- + \nu_+)[(\nu^2 + 3)\nu - (3\nu^2 + 1)/\nu_{(\text{rel})}]/[1 - \nu^2]^3 , \quad (4.8)
 \end{aligned}$$

where

$$\nu_{(\text{rel})} = (\nu_- + \nu_+)/ (1 + \nu_- \nu_+) \quad (4.9)$$

up to sign is the relativistic difference of the two velocities and vanishes when $\nu_- + \nu_+ = 0$ as occurs in the Schwarzschild case. This is a subluminal velocity only when ν_- and ν_+ are either both subluminal or both superluminal (regions A and C).

The extrema of the force function are found by examining its critical points which only exist in regions A and C where $\nu_{(\text{rel})}$ is subluminal. The critical points occur at the roots (complex in region B) of the quadratic factor in its numerator

$$\nu_{(\text{crit})\pm} = \mathcal{V}_{\pm}(\nu_{(\text{rel})}) = \left[1 \pm \sqrt{1 - \nu_{(\text{rel})}^2} \right] / \nu_{(\text{rel})} , \quad (4.10)$$

which satisfy

$$\nu_{(\text{crit})-} \nu_{(\text{crit})+} = 1 . \quad (4.11)$$

Under the assumption that $\nu_- + \nu_+ < 0$, they also satisfy $\nu_{(\text{crit})+} < -1 < \nu_{(\text{crit})-} < 0$ in region A where $-1 < \nu_{(\text{rel})} < 0$, and $0 < \nu_{(\text{crit})-} < 1 < \nu_{(\text{crit})+}$ in region C where $0 < \nu_{(\text{rel})} < 1$. Thus the only critical point in the physical region occurs at the minus root

$$\begin{aligned}
 \nu_{(\text{ext})} &= \nu_{(\text{crit})-} = \gamma_{(\text{rel})} \nu_{(\text{rel})} / (1 + \gamma_{(\text{rel})}) \\
 &\rightarrow \frac{1}{2} \nu_{(\text{rel})} \rightarrow (\nu_- + \nu_+)/2 \text{ as } \nu_{(\text{rel})} \rightarrow 0 . \quad (4.12)
 \end{aligned}$$

In region A this leads to a maximum of the force function when $\kappa < 0$ (minimum when $\kappa > 0$) and a minimum in region C when $\kappa < 0$ (maximum when $\kappa > 0$), with the extreme value

$$\mathcal{F}(\nu_{(\text{ext})}; \kappa, \nu_-, \nu_+) = \kappa [1 + (1 + \gamma_{(\text{rel})}) \nu_- \nu_+] / \gamma_{(\text{rel})} . \quad (4.13)$$

In region B there are no critical points and no extrema, but one point of inflection. $\nu_{(\text{rel})}$ has a vertical asymptote at $\nu_- \nu_+ = -1$, dividing region B into two parts: on the region A side ($\nu_- \nu_+ > -1$) it is negative as in region A, while on the region C side ($\nu_- \nu_+ < -1$) it is positive as in region C.

In region A where both ν_- and ν_+ are subluminal, the value $\nu_{(\text{ext})}$ has a simple and elegant interpretation in terms of 1-dimensional motion in special relativity. Consider three relative velocities $\nu_{\pm}, \nu_{(\text{ext})}$ of three observers with respect to a fixed fourth observer. Determine the velocity $\nu_{(\text{ext})}$ so that in its own rest frame, the

other two observers (corresponding to ν_{\pm}) have relative velocities which only differ in sign. Using the relativistic addition formula for velocities along a fixed direction, this condition is just

$$(\nu_+ - \nu_{(\text{ext})})/(1 - \nu_+ \nu_{(\text{ext})}) = -(\nu_- - \nu_{(\text{ext})})/(1 - \nu_- \nu_{(\text{ext})}) . \quad (4.14)$$

Cross-multiplying this equation leads to the same quadratic equation in $\nu_{(\text{ext})}$ as follows for ν by setting the derivative (4.8) to zero. Thus the extremal force observer sees the two oppositely rotating geodesics with the same relative speed.

It follows that the 4-velocity of the extremal velocity is just the renormalized average of the 4-velocities of the two oppositely rotating circular geodesics. This immediately yields the result

$$\nu_{(\text{ext})} = \nu_{(\text{crit})-} = [\gamma_- \nu_- + \gamma_+ \nu_+] / [\gamma_- + \gamma_+] . \quad (4.15)$$

From this and the reciprocal relation (4.11) one easily finds

$$\nu_{(\text{crit})+} = [\gamma_- \nu_- - \gamma_+ \nu_+] / [\gamma_- - \gamma_+] , \quad (4.16)$$

from which it follows that the 4-velocity of the second critical velocity is just the renormalized difference of the 4-velocities of the two oppositely rotating circular geodesics.

The geometry of the relative observer plane of the circular motion (the t - ϕ subspace of the tangent space) is very useful in visualizing the various velocities which arise here and in the spin precession analysis, and in extending this discussion to region C. For a given observer with 4-velocity u in this relative observer plane, denote the map which reflects across u by a tilde

$$U = \gamma(u + \nu \hat{e}) \rightarrow \tilde{U} = \gamma(u - \nu \hat{e}) \quad (4.17)$$

and denote by a bar the commuting map which reflects (relative to U) across the nearest forward null direction to the orthogonal direction

$$U = \gamma(u + \nu \hat{e}) \rightarrow \bar{U} = \gamma \nu (u + 1/\nu \hat{e}) , \quad (4.18)$$

where \hat{e} is a unit vector orthogonal to u in the positive ϕ direction in the relative observer plane of the circular motion. The pair (U, \bar{U}) arises from either (u, \hat{e}) or $(u, -\hat{e})$ by a boost, for a timelike future-pointing U . For the threading observers, this corresponds to the bar map introduced in Eq. (2.12). Also let $U_{\pm} = \gamma_{\pm}(u + \nu_{\pm} \hat{e})$ be the geodesic (unit) 4-velocities whenever they are not null, whether timelike or spacelike, and the same for the critical 4-velocities $U_{(\text{crit})\pm} = \gamma_{(\text{crit})\pm}(u + \nu_{(\text{crit})\pm} \hat{e})$. In regions A and C the latter pair are related to each other by the bar map because of Eq. (4.11).

Figure 5 illustrates the geometry of the various velocities in the relative observer plane of the circular motion for each of the three regions. In region A where the geodesic 4-velocities U_{\pm} are both timelike, the relative difference velocity $-\nu_{(\text{rel})} > 0$

is the (scalar) relative velocity of \tilde{U}_- with respect to U_+ . The critical velocities correspond to the 4-velocities which are the normalized sum/difference of the geodesic 4-velocities

$$\begin{aligned} \nu_{(\text{crit})\pm} &= \mathcal{V}_{\pm}(\nu_{(\text{rel})}) , \\ U_{(\text{crit})\pm}^{\alpha} &= (U_{\pm}^{\alpha} \mp U_{\mp}^{\alpha}) / \|U_{\pm} \mp U_{\mp}\| . \end{aligned} \quad (4.19)$$

In region C both U_{\pm} are spacelike. Here one may rewrite the relative velocity $\nu_{(\text{rel})} > 0$ in the following form

$$\nu_{(\text{rel})} = (\nu_-^{-1} + \nu_+^{-1}) / (1 + \nu_-^{-1} \nu_+^{-1}) , \quad (4.20)$$

revealing that its sign-reversal may be interpreted as the relative velocity of $\tilde{\tilde{U}}_-$ with respect to \tilde{U}_+ , both timelike in region C. The critical velocities now correspond to the 4-velocities which are the normalized sum/difference of the timelike barred geodesic 4-velocities or equivalently of the tachyonic four-velocities themselves

$$\begin{aligned} U_{(\text{crit})\pm}^{\alpha} &= (\bar{U}_+^{\alpha} \mp \bar{U}_-^{\alpha}) / \|\bar{U}_+ \mp \bar{U}_-\| \\ &= (U_+^{\alpha} \mp U_-^{\alpha}) / \|U_+ \mp U_-\| . \end{aligned} \quad (4.21)$$

Thus in region C the extremal observer sees the two tachyonic geodesic velocities with equal but opposite velocities as in region A.

In region B where U_+ is still timelike but U_- is spacelike, the spin-critical velocities introduced below in section 6. are determined by a similar relationship but with $\nu_{(\text{rel})}$ replaced by its reciprocal (i.e., U_- replaced by \bar{U}_-)

$$\nu_{(\text{crit,spin})\pm} = \mathcal{V}_{\pm}(1/\nu_{(\text{rel})}) = \left[1 \pm \sqrt{1 - 1/\nu_{(\text{rel})}^2} \right] \nu_{(\text{rel})} . \quad (4.22)$$

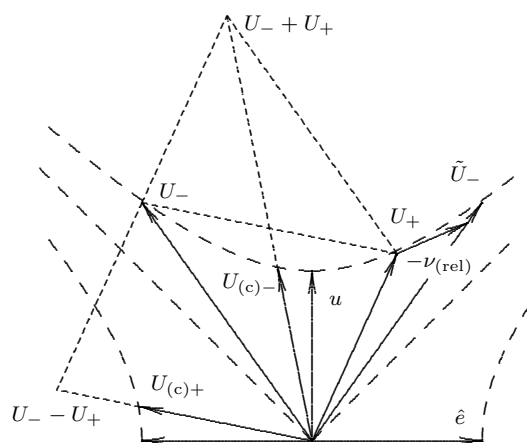
But $-\nu_{(\text{rel})}$ is the relative velocity of \tilde{U}_- with respect to U_+ and $-1/\nu_{(\text{rel})}$ is the relative velocity of $\tilde{\tilde{U}}_-$ with respect to U_+ . Therefore the corresponding spin-critical 4-velocities are related to the critical ones in the same way that the critical ones are related to the geodesic ones

$$U_{(\text{crit,spin})\pm}^{\alpha} = (U_{(\text{crit})+}^{\alpha} \mp U_{(\text{crit})-}^{\alpha}) / \|U_{(\text{crit})+} \mp U_{(\text{crit})-}\| . \quad (4.23)$$

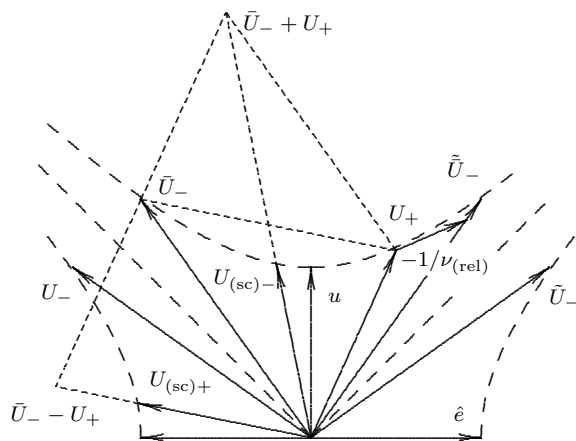
Thus if one reinterprets U_{\pm} in Figure 5(b) as the critical velocities $U_{(\text{crit})}$, then the four-velocities $U_{(\text{sc})}$ of the figure become the spin-critical velocities $U_{(\text{crit,spin})}$. A similar diagram for the region B case $\nu_- \nu_+ < -1$ has U_+ and $\tilde{\tilde{U}}_-$ interchanged relative to u .

In regions A and C one can introduce a family of ‘‘extremal force’’ observers with 4-velocity $U_{(\text{ext})}^{\alpha}$ and its associated relative velocity $\nu_{(\text{ext})}(u)^{\hat{\phi}} = \nu_{(\text{ext})}(U_{(\text{ext})}, u)^{\hat{\phi}}$ for both the Kerr and Gödel spacetimes, both of which have a pair of oppositely directed circular geodesics. The expression (4.13) with appropriate arguments then defines the acceleration of the extremal force observers. In region A their angular velocity

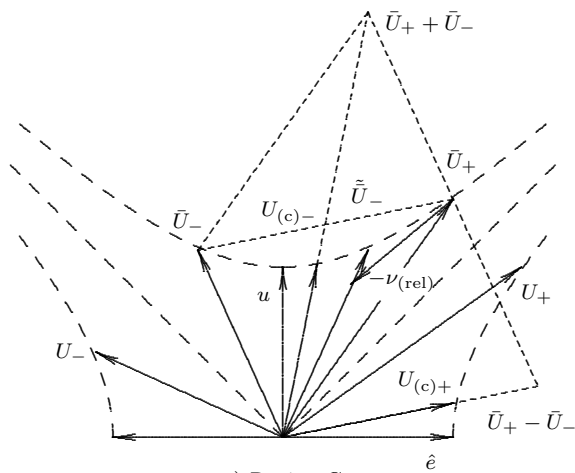
$$\zeta_{(\text{ext})} = (\Gamma_- \dot{\phi}_- + \Gamma_+ \dot{\phi}_+) / (\Gamma_- + \Gamma_+) < 0 \quad (4.24)$$



a) Region A



b) Region B ($-1 < \nu - \nu_+ < 0$)



c) Region C

Fig. 5. An illustration of the relative observer plane geometry of the various velocities which arise in the analysis of the physical radial force function for circular motion, for each of the three regions A, B, and C. In regions A and C, these determine the critical velocities (abbreviated by $U_{(c)\pm}$) of the force function directly, while in region B where the critical velocities are complex, the geometry shown instead determines the spin-critical velocities (abbreviated by $U_{(s,c)\pm}$) for the spin precession function of section 6.. The case $\nu_- \nu_+ < -1$ of region B is obtained from the case $-1 < \nu_- \nu_+ < 0$ shown in *b*) by interchanging U_+ and \tilde{U}_- , reversing the sign of the relative velocity. The case $\nu_- \nu_+ = -1$ separating these two has instead $U_+ = \tilde{U}_-$.

is easily evaluated by averaging the geodesic 4-velocities in the form (2.2), and is negative since $\Gamma_- > \Gamma_+$ as explained at the beginning of section 3.. For low speeds ($\Gamma_{\pm} \rightarrow 1$), this reduces to the average angular velocity $\zeta_{(\text{gmp})}$. In region C their angular velocity is given by the analytic continuation of above formula (Γ_{\pm} are purely imaginary so $\zeta_{(\text{ext})}$ remains real) but is instead positive.

Thus the extremal force condition picks out the family of observers which see two oppositely moving geodesic test particles symmetrically, i.e., with the same relative speed. Expressing the physical force function with respect to these observers leads to an expression which is an even function of ν since $\mathcal{F}(\nu; \kappa, -\nu_+, \nu_+) = \kappa[\nu^2 - \nu_+^2]/[1 - \nu^2]$. However, a pair of oppositely directed geodesic test particles which start from a given such observer do not return simultaneously to the same observer after each full revolution of the orbit because of the same asymmetry between corotation and counter-rotation which appears in the relationship (2.8) between the physical velocity component and the angular velocity. This is described below as a geodesic analog of the Sagnac effect.

The difference

$$\zeta_{(\text{ext})} - \zeta_{(\text{gmp})} = \frac{1}{2}[(\Gamma_- - \Gamma_+)/(\Gamma_- + \Gamma_+)][\dot{\phi}_- - \dot{\phi}_+] < 0 \quad (4.25)$$

is negative since $\Gamma_- > \Gamma_+$ and $\dot{\phi}_- < 0, \dot{\phi}_+ > 0$, so the extremal force observers counter-rotate with respect to the geodesic meeting point observers. The negative values of the angular velocities of both families of observers leading to counter-rotation with respect to the threading observers is due to the asymmetry in their equation of motion introduced by the gravitomagnetic vector force. In both cases these counter-rotate with respect to the slicing observers (which are determined by the null circular orbit meeting points) since the asymmetry introduced by the gravitomagnetic force, being proportional to the speed, is smaller for timelike velocities compared to the speed of light, and so the corotating “dragging” effect is smaller.

It seems reasonable that at least in the limit of small angular speeds, the physical force maintaining the orbits of the extremal force observers is maximum since in some sense they have the least relative angular motion with respect to the geometry, and hence require the most force to keep from falling towards the center of symmetry. This is intuitively clear in Kerr where the attraction towards the center is provided by the gravitoelectric field of the mass giving rise to the gravitational field. In the Gödel spacetime in the slicing point of view, the gravitoelectric field is also inward, so a test particle initially at rest would also begin to fall towards the axis

of symmetry as it follows a circular orbit with a different center.

Table 6. Signs of the physical component of the physical radial force and its velocity derivatives for circular orbits for the usual case $\kappa(\phi, u)^{\hat{r}} < 0$. The abbreviations $\nu_{\pm} = \nu(U_{\pm}, u)^{\hat{\phi}}$ and $\nu = \nu(U, u)^{\hat{\phi}}$ are used.

	Region A	Region B	Region C
	$\nu_- > -1$ $\nu_+ < 1$	$\nu_- < -1$ $\nu_+ < 1$	$\nu_- < -1$ $\nu_+ > 1$
$f(U)^{\hat{r}}$	positive if : $\nu_- < \nu < \nu_+$ negative if : $\nu > \nu_+$; $\nu < \nu_-$	positive if : $\nu < \nu_+$ negative if : $\nu > \nu_+$	positive
$\frac{df(U)^{\hat{r}}}{d\nu}$	any sign	negative	any sign
$\frac{d^2 f(U)^{\hat{r}}}{d\nu^2}$	negative	any sign	positive

Table 6 gives the sign of the physical force and of its first and second derivatives for each of these regions. For the Gödel spacetime, there is always at least one timelike geodesic at every radius (the threading observers) so region C does not exist, while region C disappears from the Kerr spacetime in the extreme case $a = \mathcal{M}$. Similarly the region B, whose existence is due to the asymmetry in the angular motion introduced by the rotation of the reference frame, disappears in the Schwarzschild limit $a = 0$ of Kerr. In the rotating Minkowski spacetime, the two real roots of the force function coincide, so there is only one circular geodesic (the counter-rotating slicing observer) and it is timelike at each radius where the threading point of view is valid, so only region A exists in both points of view. Figure 4 shows the dependence of the radius r as a function of a for Kerr for the two boundaries $r_{(AB)}$, $r_{(BC)}$ between the three regions A, B, and C, together with the radii of the relatively straight circles and embedding-signature-switching circles for the threading point of view discussed in the appendix.

For each value of the radial variable, one can plot the physical force $f(U)^{\hat{r}}$ versus the physical component $\nu(U, u)^{\hat{\phi}}$ of the relative velocity in the angular direction for both the threading and slicing points of view. Figure 6 shows a representative sample of these curves for the rotating Minkowski spacetime, the Gödel spacetime, the Kerr spacetime with $a/\mathcal{M} = 0.5$, and the Schwarzschild spacetime $a = 0$. Shown also is the curve whose intersection with each force graph occurs at the velocity of the other family of observers. In the Gödel slicing case, for example, this is just the positive horizontal axis since the threading observers are geodesic and corotating. The curves of relative extrema of the force graphs are also plotted.

Note that in the slicing point of view in Minkowski spacetime, only the space curvature force due to the circular orbit is nonzero. This is just the usual inward centripetal acceleration required to maintain a circular orbit under the influence of no real forces, scaled by a squared gamma factor. It has a maximum at the relative velocity of the slicing observers, which are the extremal force observers in this case.

Increasing the radius flattens the force graph due to its inverse dependence on r . In the threading point of view, the force graph also migrates to the left as it follows the velocity of the single counter-rotating circular geodesic followed by the slicing observers at each radius, going infinite at the threading observer horizon radius.

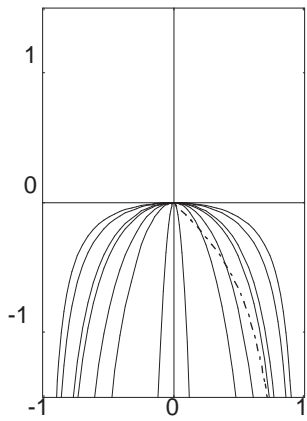
For a rotating spacetime the physical force $f(U)^{\hat{r}}$ is not a symmetric function of the relative velocity $\nu(U, u)^{\hat{\phi}}$ since the gravitomagnetic vector force introduces an asymmetry between the corotating and counter-rotating orbits. For the Kerr and Gödel spacetimes the maxima and minima of the force graphs in regions A and C do not occur at zero velocity. At these extrema the derivative of the force with respect to the velocity changes sign at a nonzero relative velocity, leading to effects which run counter to our ordinary Newtonian intuition about the radial force for circular orbits in a force field.

For those spacetimes with a region A (Kerr and Gödel), the sign of the radial force in that region behaves according to our Newtonian intuition about circular orbits. A positive (outward) radial force is required to support a circular orbit with speed less than the Keplerian speed, and a negative (inward) force is required to hold in a circular orbit with more than that speed. In the Schwarzschild case, the extrema of the force graphs occur at zero velocity and are local maxima in this region, so increasing the speed decreases the outward radial force needed to maintain the orbit. However, for the Kerr and Gödel spacetimes, the local maxima occur at negative (slicing or threading) velocities, so for the counter-rotating orbits between zero velocity and the one at the local maximum, increasing the speed increases the outward radial force necessary to maintain the orbit, which is the opposite of what happens in Newtonian gravity. We refer to this simply as “counter-intuitive radial force behavior.” Thus in region A, extending to infinite radius in Kerr but from zero radius out to the radius at which the counter-rotating geodesic becomes spacelike in the Gödel spacetime, those counter-rotating orbits with speeds less than the speed at which the maximum of the force occurs experience this behavior.

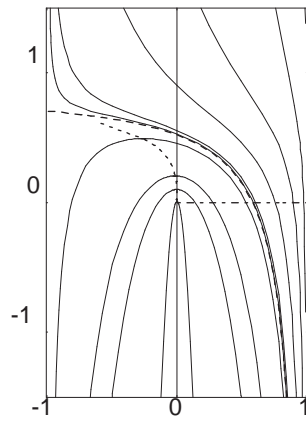
For those spacetimes with a region B (Kerr and Gödel) where only the counter-rotating geodesic is spacelike (superluminal velocity), there is no local extremum on each force graph in this region. A particle on a counter-rotating circular orbit is forced to move with a velocity smaller than the (unphysical) geodesic speed and so it must be pushed outward (positive force) to maintain the orbit. This is as expected. However, if the speed of a counter-rotating orbit increases then the positive force increases as well, which is again counterintuitive.

In the region C in the Kerr spacetime where both the corotating and the counter-rotating circular geodesics are spacelike (superluminal velocities), both corotating and counter-rotating test particles are forced to move with a speed less than the geodesic speed thus always yielding a positive (outward) radial force. As their speed approaches 1, the Lorentz gamma factor goes to infinity causing the physical force to increase to infinity as well. Since a local minimum occurs at a corotating (positive) velocity, increasing the speed increases the outward force for velocities outside the interval between zero velocity and the positive velocity where the minimum occurs.

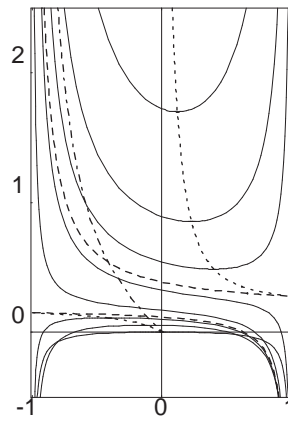
(a) Minkowski: Sli



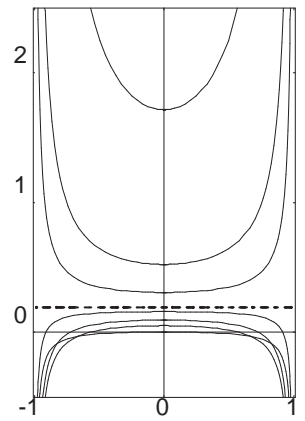
(b) Godel: Sli



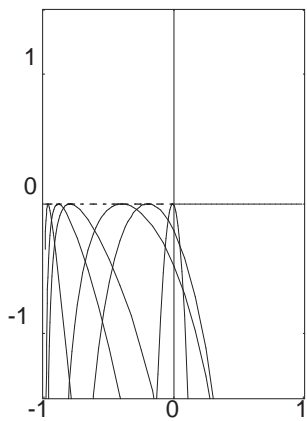
(c) Kerr: Sli



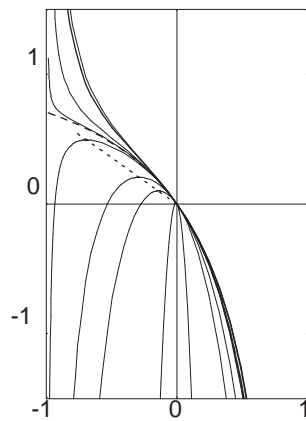
(d) Schwarzschild



(e) Minkowski: Thd



(f) Godel: Thd



(g) Kerr: Thd

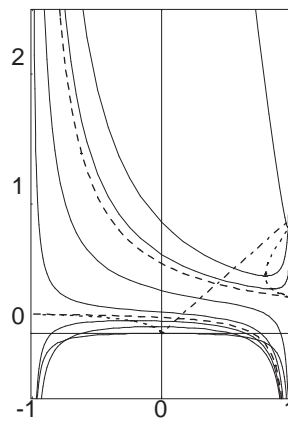


Fig. 6. f versus ν : plots of the radial physical component of the force acting on a nonzero rest mass test particle moving on an equatorial circular orbit as a function of the physical component of the relative velocity of the particle in the angular direction for the rotating Minkowski, Gödel, Kerr ($a/\mathcal{M} = 0.5$), and Schwarzschild ($a = 0$) spacetimes. The solid curves are the graphs of the force plotted versus the relative velocity for selected values of the radius. For the spacetimes other than rotating Minkowski, regions A, B, and C are the regions which are separated by the long dashed lines, from bottom to top. Region C is missing in Gödel and region B in Schwarzschild. The short dashed lines connect the local extrema of the force graphs. The long-short dashed line marks the point on a given such graph which occurs at the velocity of the other family of observers. For Kerr the force curves move higher along the vertical axis with decreasing radius from region A extending out to infinity through region B into region C containing the ergosphere and finally approaching the observer horizon. This is also true for Schwarzschild except that region B disappears between the interface of regions A and C at $r = 3m$. For Gödel they move higher along the vertical axis (slicing diagram) or the dashed-dotted line (threading diagram) with increasing radius from region A near $r = 0$ into region B approaching the observer horizons. For the rotating Minkowski slicing diagram, they move outward from the vertical axis with increasing radius, and in the threading diagram they move to the left with increasing radius toward the observer horizon. The thickened force curve represents the radius of the ergosphere (threading observer horizon) in the Kerr slicing case and the corresponding slicing observer horizon radius in the Gödel threading case. Almost no change in the force curve occurs beyond that radius in the Gödel threading case.

Thus some corotating and all counter-rotating orbits exhibit counter-intuitive radial force behavior.

This happens for all circular orbits in region C in the Schwarzschild spacetime, where the interval between zero velocity and the velocity of this minimum shrinks to zero width. The corotating and counter-rotating geodesic velocities take the relativistically corrected Keplerian values

$$\nu(U_{\mp}, u)^{\hat{\phi}} = \mp \sqrt{\mathcal{M}/r} / \sqrt{1 - 2\mathcal{M}/r} \quad (4.26)$$

and the physical force reduces to

$$f(U)^{\hat{r}} = \kappa(\phi, u)^{\hat{r}} \gamma(U, u)^2 [(\nu(U, u)^{\hat{\phi}})^2 - (\nu(U_{\mp}, u)^{\hat{\phi}})^2], \quad (4.27)$$

where the signed relative curvature is

$$\kappa(\phi, u)^{\hat{r}} = -\sqrt{1 - 2\mathcal{M}/r}/r. \quad (4.28)$$

The two circular geodesics become null at $r = 3\mathcal{M}$ where $|\nu(U_{\mp}, u)^{\hat{\phi}}| = 1$, and then spacelike for smaller radii. At this coordinate radius the physical force reduces to $f(U)^{\hat{r}} = -\kappa(\phi, u)^{\hat{r}} > 0$ which is independent of the velocity of the test particle, leading to the dashed line force graph separating the two regions A and C in Figure 6(d). For $2\mathcal{M} < r < 3\mathcal{M}$ (region C), the circular geodesics are both spacelike and the physical force on the test particle must be positive. Moreover $f(U)$ is an increasing function of $|\nu(U, u)^{\hat{\phi}}|$ in that region and so increasing the speed of the test particle increases the outward physical force, contrary to Newtonian intuition.

This counter-intuitive radial force behavior was first discovered by Abramowicz^{12,13} in the Schwarzschild case inside $r = 3\mathcal{M}$, the outer boundary in the equatorial plane of his “rotosphere”,¹³ and he explains it as due to a reversal of

the “optical centrifugal force” in a decomposition of the physical force into a sum of terms. de Felice^{27,28} has noticed this behavior in the Kerr spacetime using a factorization of the physical force in terms of angular velocity, which is closely connected to the threading point of view relative velocity, and he uses the term “prehorizon regime” to characterize it, since initially he interpreted this behavior as a way of signaling the approach to a horizon. Later he discovered that it can occur for counter-rotating orbits even a great distances from a rotating object.³¹ Barrabès, Boisseau, and Israel³⁴ have used the hypersurface point of view to describe the same phenomenon for both Schwarzschild and Kerr, but using a factorization of the physical force in terms of the slicing relative velocities.

Of course all of these effects depend on the zero point used for the relative speed, and are therefore observer-dependent. The choice of observer used to describe the effect depends on exactly what one wants to measure or explain. The threading point of view is relevant to behavior as seen from infinity, while the hypersurface point of view might be appropriate for local considerations like accretion disks. For the extremal force observers in region A introduced above, the extrema of the physical force occur at zero relative velocity. A similar family exists in region C. For example, in the region C of the Kerr diagram, one sees that the corotating family of observers for which the minimum occurs approaches the slicing observers at the horizon but increasingly corotates faster than those observers until it experiences its own outer observer horizon as one moves out to the radius of the corotating photon orbit. In this region C the counter-intuitive radial force behavior occurs for all relative velocities with respect to these observers just as in the Schwarzschild case. For a certain interval of larger radii (region B), no extremum occurs. Then in the region A outside the radius at which the counter-rotating photon orbit occurs, one has a counter-rotating family for which the maxima occur. This second family has an inner horizon at that radius and counter-rotates with respect to the threading observers but approaches them at infinite radius. For this second family the counter-intuitive radial force behavior does not occur. Figure 7(a) shows the coordinate angular velocity of each of the geometrically defined observer families for the Kerr spacetime as a function of the radius (see Fig. 2 of de Felice and Usseglio-Tomasset²⁸), including the Carter family associated with the usual orthogonal frame in which the Kerr metric is stated in Boyer-Lindquist coordinates (Eq. (33.2) of Misner, Thorne, and Wheeler³⁸), an observer family which has a coordinate angular velocity $\zeta_{(\text{car})} = a/(r^2 + a^2)$ and simultaneously diagonalizes the electric and magnetic parts of the curvature tensor. Figure 7(b) shows the corresponding plot of the observers’ physical relative velocities in the slicing point of view.

Finally consider the less usual case in which the Lie signed relative curvature is positive, $\kappa(\phi, u)^{\hat{r}} > 0$, which would seem to reverse the sign of the physical force as one crosses the Lie relatively straight trajectory from the side for which $\kappa(\phi, u)^{\hat{r}} < 0$. However, the superluminal velocity $\nu(U_-, u)$ blows up at this radius, switching signs so that the physical force remains finite and does not change sign, even though the relative centripetal acceleration itself does change sign (“reversal of

the centrifugal force” in the language of Abramowicz et al,¹² but in the true relative geometry rather than the optical one). For example, in the extreme Kerr case in the threading point of view, the relative curvature becomes positive for $r < r_{(\text{rs})}$ and the space curvature force along the corotating circular orbit becomes negative while $\nu(U_-, m)^{\hat{r}}$ blows up there. In the Gödel spacetime this instead occurs in the slicing point of view where the relative curvature becomes positive for $r > r_{(\text{rs})}$.

5. Optical geometry and inertial forces in the static case

The preceding companion article [BCJ1] shows how the optical gauge conformal transformation of the spatial metric changes the relative centripetal acceleration to the optical relative centripetal acceleration and reshuffles the various spatial forces in the spatial equation of motion. As discussed there, the optical geometry is only natural in the static case, which in the present context applies to the Schwarzschild limit of the Kerr spacetime.

Those results are easily specialized to this latter case, so that one can see how the various radial spatial forces for circular orbits are transformed under the conformal transformation. Agreeing that orthonormal components of optical quantities are normalized in the optical geometry, the transformation of the signed Lie relative curvature (equation (14.3) of [BCJ1]) is

$$\tilde{\kappa}(\phi, u)^{\hat{r}} = \sigma^{-1}[\kappa(\phi, u)^{\hat{r}} - (\ln \sigma)_{,\hat{r}}] , \quad (5.1)$$

while the curvatures themselves are

$$\tilde{\kappa}(\phi, u)^{\hat{r}} = -(1 - 3\mathcal{M}/r)/r , \quad \kappa(\phi, u)^{\hat{r}} = -(1 - 2\mathcal{M}/r)^{1/2}/r . \quad (5.2)$$

With the static relation $g(u)^{\hat{r}} = (\ln \sigma)_{,\hat{r}}$ that follows from the optical choice $\sigma = M^{-1}$ or $\sigma = N^{-1}$ respectively, this leads to equation (A.23) of [BCJ1] for the transformation of the centripetal acceleration, here specialized to orthonormal components

$$\sigma^{-1}\tilde{a}_{(\text{tem})}^{(\perp)}(U, u)^{\hat{r}} = a_{(\text{tem})}^{(\perp)}(U, u)^{\hat{r}} - |\nu(U, u)^{\hat{\phi}}|^2 g(u)^{\hat{r}} . \quad (5.3)$$

For comparison with the literature, note that the conformal factor is not present in the covariant (unnormalized) coordinate component form of this equation.

Using this result in equation (4.2), one finds the following expression for the physical force necessary to maintain the circular orbit in terms of the Lie optical relative acceleration

$$\begin{aligned} f(U)^{\hat{r}} &= \sigma^{-1}\gamma(U, u)^2\tilde{a}_{(\text{lie})}^{(\perp)}(U, u)^{\hat{r}} - \gamma(U, u)F_{(\text{lie})}^{(\text{G})}(U, u)^{\hat{r}} + \gamma(U, u)^2|\nu(U, u)^{\hat{\phi}}|^2 g(u)^{\hat{r}} \\ &= \sigma^{-1}\gamma(U, u)^2\tilde{a}_{(\text{lie})}^{(\perp)}(U, u)^{\hat{r}} - g(u)^{\hat{r}} , \end{aligned} \quad (5.4)$$

where the extra term $\gamma(U, u)^2|\nu(U, u)^{\hat{\phi}}|^2 g(u)^{\hat{r}}$ which comes from the conformal transformation of the centripetal acceleration combines with the term $-\gamma(U, u)^2 g(u)^{\hat{r}}$ in the spatial gravitational force to form a velocity-independent force, namely minus the gravitoelectric field $-g(u)^{\hat{r}}$. Abramowicz refers to this as the gravitational

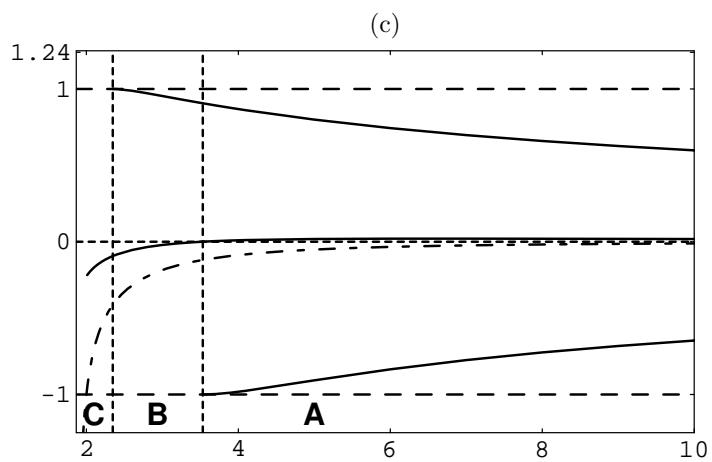
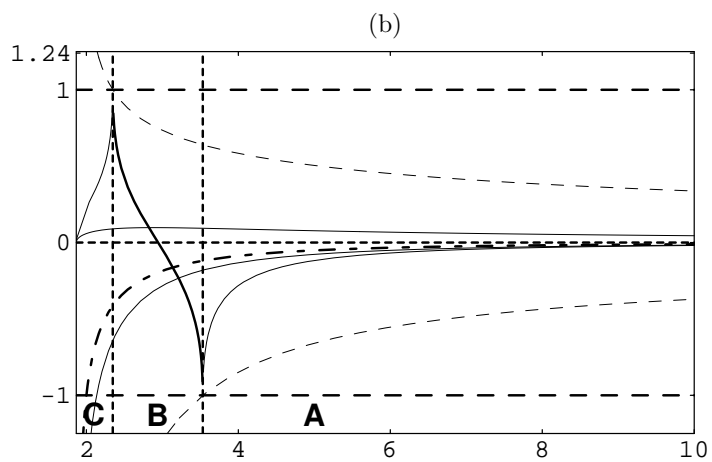
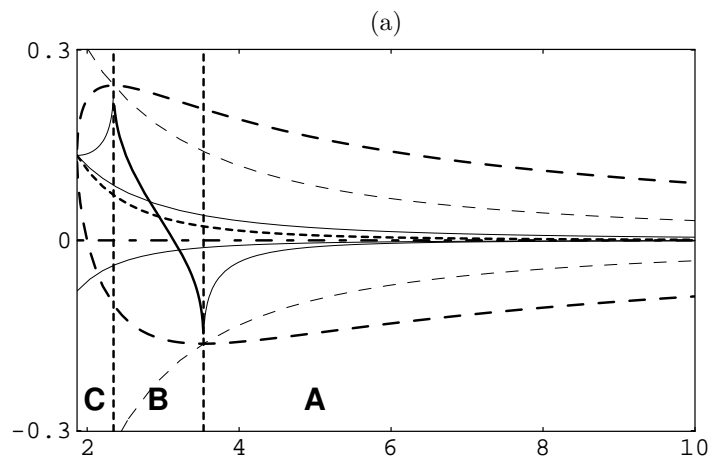


Fig. 7. (a). ζ versus \bar{r} : plots of the coordinate angular velocities of the preferred observer families in the equatorial plane of the Kerr spacetime as a function of the radial coordinate \bar{r} for $\bar{a} = 0.5$. The thick outer long dashed curves (ζ_+ above, ζ_- below) correspond to the null orbits which enclose the physical region of timelike orbits, a region divided in two by the thick short dashed curve $\zeta_{(\text{sli})}$; these three curves meet at the horizon at the left edge of the graph. The thick long-short dashed horizontal axis corresponds to $\zeta_{(\text{thd})} = 0$. The two solid curves immediately above and below $\zeta_{(\text{sli})}$ and $\zeta_{(\text{thd})} = 0$ respectively are $\zeta_{(\text{car})}$ and $\zeta_{(\text{gmp})}$. The thin dashed curves are $\zeta_{(\text{geo})\pm} = \dot{\phi}_{\pm}$, which intersect the null orbit curves at the interface between regions A, B, and C by definition. The solid curves in regions A and C terminating in these same intersection points correspond to ($\zeta_{(\text{ext})}$). The curve decreasing from the upper geodesic photon point to the lower geodesic photon point in region B is $\zeta_{(\text{crit,spin})}$ where the threading precession is extremal.

(b). ν versus \bar{r} : the plot of the corresponding physical relative velocities in the slicing point of view as a function of the radius.

(c). ν versus \bar{r} : the same plot as in (b) showing the three physical relative velocities at which the corrected spin precession $\zeta(U, m, E)^{\hat{z}}$ vanishes.

force,²⁰ but with respect to the local rest space of the test particle itself, not the static observers fixed in the geometry of the spacetime.

The remaining term in the physical force, namely the sign reversal of the Lie optical relative centripetal acceleration multiplied by the proper time correction factor $\gamma(U, u)^2$ and the conformal transformation factor for relative acceleration, is what Abramowicz identifies as his centrifugal force in the static case. The Lie optical relative centripetal acceleration is (see [BCJ1]) is explicitly

$$\tilde{a}_{(\text{lie})}^{(\perp)}(U, u)^{\hat{r}} = -|\tilde{\nu}(U, u)^{\hat{\phi}}|^2 [\ln \tilde{g}(u)_{\phi\phi}^{1/2}]_{,\hat{r}} , \quad (5.5)$$

where $\tilde{\nu}(U, u)^{\hat{r}} = \sigma\nu(U, u)^{\hat{r}}$. In their attempts to extend Abramowicz's work to the Kerr spacetime, Iyer and Prasanna^{19, 25, 26} evaluate this result for the slicing decomposition, while Prasanna and Chakrabarti¹⁸ evaluate it for the threading decomposition, modulo conformal factors.

The step which goes from the spatial equation of motion expressed in terms of the sum of the relative centripetal acceleration and the spatial gravitoelectric force to the same equation expressed in terms of the sum of the optical relative centripetal acceleration and the Abramowicz gravitational force in the Schwarzschild case is explicitly

$$\begin{aligned} f(U)^{\hat{r}} &= \left[-\gamma(U, u)^2 |\nu(U, u)^{\hat{\phi}}|^2 \frac{r - 2\mathcal{M}}{r^2} + \gamma(U, u)^2 \frac{\mathcal{M}}{r^2} \right] (1 - 2M/r)^{-1/2} \\ &= \left[-\gamma(U, u)^2 |\nu(U, u)^{\hat{\phi}}|^2 \frac{r - 3\mathcal{M}}{r^2} + \frac{\mathcal{M}}{r^2} \right] (1 - 2M/r)^{-1/2} . \end{aligned} \quad (5.6)$$

This clearly shows the result that at $r = 3\mathcal{M}$, the physical force acting on the test particle is independent of its velocity. This last property of the physical force is lost in the corresponding stationary case because of the presence of the velocity-dependent gravitomagnetic force.

6. Spin precession

A test gyroscope following a test particle world line in spacetime undergoes Fermi-Walker transport along that worldline. Precession of the spin direction is a relative effect, depending on both the family of test observers and the single test observer following the test particle world line. Spin precession for geodesic motion will be analyzed first, and then followed by the case of accelerated motion. Papapetrou⁴⁴ has shown that a spinning particle does not follow a geodesic in spacetime but is subject to Riemannian tensor forces. These forces and any non-gravitational forces acting on a gyroscope are represented by the force $F(U, u)^\alpha$, which leads to the Thomas precession term given below for accelerated motion.

The precession angular velocity of the spin of a gyroscope (with 4-velocity U^α) as seen in its own local rest space is a relative effect, parametrizing the derivative of the relative boost between the local rest space of an observer congruence and the local rest space of the gyroscope along its world line. Given an observer-adapted orthonormal spatial frame $\{E_a^\alpha\}$ on spacetime which is tied to the observer congruence by spatial co-rotating Fermi-Walker transport, one can boost the frame to the local rest space of the gyroscope, and the components of its spin with respect to that boosted frame will undergo a time-dependent rotation with an associated proper time angular velocity having components

$$\zeta(U, u, E)^a = \gamma(U, u)[\zeta_{(\text{cfw})}(U, u)^a + \zeta_{(\text{sc})}(U, u, E)^a], \quad (6.1)$$

where

$$\begin{aligned} \zeta_{(\text{cfw})}(U, u)^a &= -\frac{1}{2}H(u)^a \\ &\quad -\gamma(U, u)[\gamma(U, u) + 1]^{-1}[\nu(U, u) \times_u F(U, u)]^a \\ &\quad +[\gamma(U, u) + 1]^{-1}[\nu(U, u) \times_u F_{(\text{fw})}^{(\text{G})}(U, u)]^a \\ &= \zeta_{(\text{gm})}(u)^a + \zeta_{(\text{thom})}(U, u)^a + \zeta_{(\text{geo})}(U, u)^a \end{aligned} \quad (6.2)$$

is the precession angular velocity relative to a spatial (with respect to u^α) co-rotating Fermi-Walker frame transported along U^α (and consisting of gravitomagnetic, Thomas, and geodesic terms), while the space curvature term

$$\zeta_{(\text{sc})}(U, u, E)^a = \frac{1}{2}\eta(u)^{abc}\Gamma(u)_{[b|d|c]}\nu(U, u)^d \quad (6.3)$$

is the relative angular velocity of the latter frame with respect to the observer-adapted frame $\{E_a^\alpha\}$, and the factor $\gamma(U, u)$ in Eq. (6.1) is necessary to convert the observer proper time derivative to the gyroscope proper time derivative. Conversely, removing the gamma factor in Eq. (6.1) one obtains the precession of the spin as seen by the sequence of observers along its path, removed of the directional distortions caused by the Lorentz boost between the two local rest spaces.

This description is valid for an arbitrary spacetime.⁵ For the threading observers in the nonlinear reference frame associated with post-Newtonian coordinates in that approximation to general relativity, one obtains the Schiff formula for the precession

with respect to the “distant stars.” One can use those same general results in the threading point of view for any of the three spacetimes under consideration to obtain an exact precession formula for a gyroscope in an equatorial plane circular orbit. The natural observer-adapted (right-handed) orthonormal spatial frame E_a^α which is tied to the threading observer congruence by corotating Fermi-Walker transport (in the equatorial plane) consists of unit vectors along the coordinate radial r direction, the observer local rest space ϕ direction, and the $-\theta$ or positive z direction, respectively. The relative observer boost of this spatial frame to the local rest space of the gyro, completed to a spacetime frame by the gyro 4-velocity, is called a phase-locked frame by de Felice and Usseglio-Tomasset^{32,33} who investigate the Kerr case, and it is also the spacetime Serret-Frenet frame for the circular orbit discussed in detail by Iyer and Vishveshwara,³⁶ who treat the general stationary axisymmetric case.

For Kerr, the resulting spin precession formula has the same interpretation as the Schiff formula, namely the precession of the spin with respect to a local frame locked onto the distant stars. For the Gödel spacetime, one obtains the precession with respect to a local frame locked into the perfect fluid source of the gravitational field, which reduces to the gravitomagnetic term alone in the corotating geodesic case where the relative velocity is zero. For the rotating Minkowski spacetime, the circular geodesics correspond to points fixed in the inertial coordinates of the slicing observers, so the precession question is not interesting without considering accelerated circular orbits, where the Thomas precession is obtained in the slicing point of view.⁵ In all cases the only nonvanishing component of the spin precession is

$$\begin{aligned}\zeta(U, m, E)^{\hat{z}} &= \gamma(U, m)[\zeta_{(\text{cfw})}(U, m)^{\hat{z}} + \zeta_{(\text{sc})}(U, m, E)^{\hat{z}}] \\ &= \gamma(U, m)\zeta_{(\text{sph})}(U, m, E)^{\hat{z}},\end{aligned}\quad (6.4)$$

where $\zeta_{(\text{sph})}(U, m, E)^{\hat{z}}$ is the precession of the spin with respect to the static spherical frame as seen by the sequence of observers along the gyro world line.

First consider the case of geodesic motion so that the Thomas precession is zero. For an equatorial circular geodesic in an axisymmetric stationary spacetime, the angular velocity terms in the threading point of view take the form

$$\zeta_{(\text{cfw})}(U, m)^{\hat{z}} = -\frac{1}{2}H(m)^{\hat{z}} - \frac{\nu(U, m)^{\hat{\phi}}}{\gamma(U, m) + 1}F_{(\text{fw})}^{(\text{G})}(U, m)^{\hat{r}},\quad (6.5)$$

where

$$F_{(\text{fw})}^{(\text{G})}(U, m)^{\hat{r}} = \gamma(U, m)[g(m)^{\hat{r}} + \frac{1}{2}\nu(U, m)^{\hat{\phi}}H(m)^{\hat{z}}],\quad (6.6)$$

and

$$\begin{aligned}\zeta_{(\text{sc})}(U, m, E)^{\hat{z}} &= -\frac{1}{2}\nu(U, m)^{\hat{\phi}}(\ln \gamma_{\phi\phi})_{,\hat{r}} = \nu(U, m)^{\hat{\phi}}\kappa(\phi, m)^{\hat{r}} \\ &= \nu(U, m)^{\phi} \text{sgn}(\kappa(\phi, m)^{\hat{r}}) R(m)/\rho(\phi, m),\end{aligned}\quad (6.7)$$

where $R(m) = \gamma_{\phi\phi}^{1/2}$.

For the Kerr spacetime the relative velocities and gamma factors of the circular geodesics are

$$\begin{aligned}\nu(U_{\pm}, m)^{\hat{\phi}} &= \sqrt{\Delta}/[a \pm \sqrt{r/\mathcal{M}}(r - 2\mathcal{M})], \\ \gamma(U_{\pm}, m) &= \left(1 - \frac{2\mathcal{M}}{r} \pm a\sqrt{\frac{\mathcal{M}}{r^3}}\right) \left[\left(1 - \frac{2\mathcal{M}}{r}\right)\left(1 - \frac{3\mathcal{M}}{r} \pm 2a\sqrt{\frac{\mathcal{M}}{r^3}}\right)\right]^{-1/2},\end{aligned}\quad (6.8)$$

and the gravitomagnetic, geodesic, and space curvature angular velocities are

$$\begin{aligned}\zeta_{(\text{gm})}(m)^{\hat{z}} &= -\frac{a\mathcal{M}}{r^2(r - 2\mathcal{M})}, \\ \zeta_{(\text{geo})}(U_{\pm}, m)^{\hat{z}} &= -\frac{\mathcal{M}\gamma(U_{\pm}, m)\nu(U_{\pm}, m)^{\hat{\phi}}(-\sqrt{\Delta} + a\nu(U_{\pm}, m)^{\hat{\phi}})}{(\gamma(U_{\pm}, m) + 1)r^2(r - 2\mathcal{M})} \\ &= \pm \frac{\gamma(U_{\pm}, m) - 1}{\gamma(U_{\pm}, m)} \sqrt{\frac{\mathcal{M}}{r^3}}, \\ \zeta_{(\text{sc})}(U_{\pm}, m, E)^{\hat{z}} &= -\frac{\nu(U_{\pm}, m)^{\hat{\phi}}[r(r - 2\mathcal{M})^2 - \mathcal{M}a^2]}{\sqrt{\Delta}r^2(r - 2\mathcal{M})} \\ &= \frac{a\mathcal{M}}{r^2(r - 2\mathcal{M})} \mp \sqrt{\frac{\mathcal{M}}{r^3}},\end{aligned}\quad (6.9)$$

The sum of these three terms

$$\begin{aligned}\zeta_{(\text{sph})}(U_{\pm}, m, E)^{\hat{z}} &= \zeta_{(\text{gm})}(m)^{\hat{z}} + \zeta_{(\text{geo})}(U_{\pm}, m)^{\hat{z}} + \zeta_{(\text{sc})}(U_{\pm}, m, E)^{\hat{z}} \\ &= \mp \gamma(U_{\pm}, m)^{-1} \sqrt{\frac{\mathcal{M}}{r^3}}\end{aligned}\quad (6.10)$$

gives the total precession angular velocity of the spin with respect to the spherical static frame in terms of the threading observer proper time. It vanishes in the limit $\gamma(U_{\pm}, m)^{-1} \rightarrow 0$ as $|\nu(U_{\pm}, m)| \rightarrow 1$ which occurs for the two freefall photon orbits, corresponding to a locking of the spin to that frame. This is consistent with the picture of a photon as a massless spinning particle with spin along the direction of motion, i.e., locked to the $\hat{\phi}$ -direction in the case of a circular orbit. On the other hand, the precession from the point of view of the gyro has the same simple form $\zeta(U_{\pm}, m, E)^{\hat{z}} = \mp \sqrt{\mathcal{M}/r^3}$ as in the Schwarzschild limit.

However, since the static spherical frame is locked to the radial direction, it undergoes a rotation of $2\pi \text{sgn} \nu(U, n)^{\hat{\phi}}$ during each revolution with respect to Cartesian-like frames along the gyro worldline and so the spin rotates an additional $-2\pi \text{sgn} \nu(U, n)^{\hat{\phi}}$ with respect to the Cartesian-like frames. This corresponds to a precession angular velocity of the spherical frame components of the spin of the gyroscope equal to the orbital coordinate angular velocity which must therefore be added to the space curvature precession to correct it, once suitably scaled to account for the difference between coordinate and observer proper times

$$d\phi_{\pm}/d\tau_{(U_{\pm}, m)} = \nu(U_{\pm}, m)^{\hat{\phi}} = \pm \sqrt{\frac{\mathcal{M}}{r^3}} \sqrt{1 - \frac{2\mathcal{M}}{r}} / \left[1 - \frac{2\mathcal{M}}{r} \pm a\sqrt{\frac{\mathcal{M}}{r^3}}\right]. \quad (6.11)$$

The corrected space curvature angular velocity is then

$$\begin{aligned}
 \zeta_{(\text{sc,cor})}(U_{\pm}, m, E)^{\hat{z}} &= \zeta_{(\text{sc})}(U_{\pm}, m, E)^{\hat{z}} + \nu(U_{\pm}, m)^{\phi} \\
 &= [1 + \text{sgn}(\kappa(\phi, m)^{\hat{r}})R(m)/\rho(U_{\pm}, m)]\nu(U_{\pm}, m)^{\phi} \\
 &= \frac{a\mathcal{M}}{r^2(r-2\mathcal{M})} \mp \sqrt{\frac{\mathcal{M}}{r^3}} \left(1 - \frac{\sqrt{1 - \frac{2\mathcal{M}}{r}}}{1 - \frac{2\mathcal{M}}{r} \pm a\sqrt{\frac{\mathcal{M}}{r^3}}} \right).
 \end{aligned} \tag{6.12}$$

For $r > r_{(\text{rs})}$ when $\text{sgn}(\kappa(\phi, m)^{\hat{r}}) < 0$, this reduces to $[\Delta(m)/2\pi]\nu(U_{\pm}, m)^{\phi}$, where the quantity the quantity $\Delta(m)$ is the deficit angle of the tangent cone to the embedding of the r - ϕ coordinate surface (with the threading geometry) in E_3 , as explained in the appendix. Thus Thorne's conical deficit argument using the threading embedding space⁵¹ holds exactly in this region.

The total precession angular velocity of the gyroscope with respect to the distant stars can then be written

$$\begin{aligned}
 \zeta_{(\text{cor})}(U_{\pm}, m, E)^{\hat{z}} &= \gamma(U_{\pm}, m)[\zeta_{(\text{gm})}(m)^{\hat{z}} + \zeta_{(\text{geo})}(U_{\pm}, m)^{\hat{z}} + \zeta_{(\text{sc,cor})}(U_{\pm}, m, E)^{\hat{z}}] \\
 &= \mp \sqrt{\frac{\mathcal{M}}{r^3}} [1 - (1 - \frac{3\mathcal{M}}{r} \pm 2a\sqrt{\frac{\mathcal{M}}{r^3}})^{-1/2}].
 \end{aligned} \tag{6.13}$$

Figure 8 shows the gravitomagnetic, geodesic, and corrected space curvature angular velocity for extreme Kerr as functions of r/\mathcal{M} .

Table 7. The spin precession $\zeta(U, m)^{\hat{z}}$ terms for geodesic circular orbits, including low speed limits indicated by arrows. The abbreviation $\gamma_- = \gamma(U_-, m)$ is used. Note that $\gamma_- = C(1 - S^2)^{-1/2}$ in the Gödel case.

	Rotating Minkowski : U_-	Gödel: U_-	Kerr : U_{\pm}
$\zeta_{(\text{gm})}^{\hat{z}}$	$-\Omega\gamma^2 \rightarrow -\Omega$	$-\Omega$	$\rightarrow -\frac{a\mathcal{M}}{r^3}$
$\zeta_{(\text{geo})}^{\hat{z}}$	0	$-\Omega[1 - \gamma_-^{-1}] \rightarrow 0$	$\rightarrow \pm \frac{1}{2} \sqrt{\frac{\mathcal{M}^3}{r^5}}$
$\zeta_{(\text{sc,cor})}^{\hat{z}}$	$\Omega\gamma_-[\gamma_- - 1] \rightarrow 0$	$2\Omega[1 - 1/C] \rightarrow 0$	$\rightarrow \pm \sqrt{\frac{\mathcal{M}^3}{r^5}}$
$\zeta_{(\text{cor})}^{\hat{z}}$	$-\Omega$	$\Omega[1 - 2/\sqrt{1 - S^2}] \rightarrow -\Omega$	$\rightarrow [\pm \frac{3}{2} - \frac{a/\mathcal{M}}{\sqrt{\mathcal{M}/r}}] \sqrt{\frac{\mathcal{M}^3}{r^5}}$

Table 7 summarizes the corresponding results for the rotating Minkowski and Gödel spacetimes, including their small r (low relative velocity) limits. This table also lists the small \mathcal{M} , small a limits for Kerr for comparison. These latter expressions agree with the well known post-Newtonian results. but it is important to note that the geodesic term in the precession formula and the corrected space curvature term, arising from very different phenomena in the strong field case, combine to form the single ‘‘geodetic precession’’ term in this weak field limit. For the counter-rotating circular geodesics in rotating Minkowski spacetime, the precession corresponds to the rotation of the inertial coordinate axes with respect

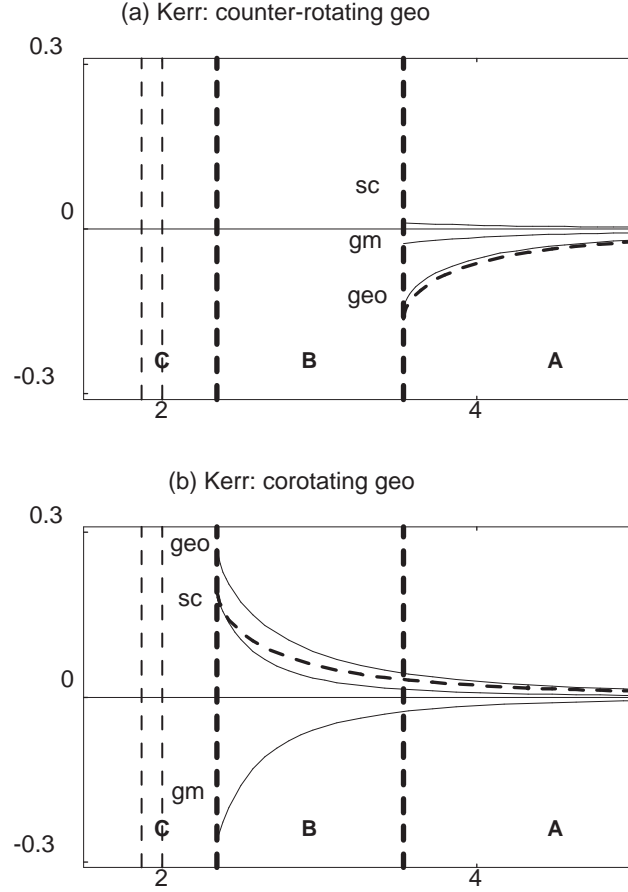


Fig. 8. ζ versus \bar{r} : plots of the geodesic, space curvature (corrected), and gravitomagnetic precession angular velocity of the spin of a gyroscope moving on (a) counter-rotating and (b) corotating equatorial circular geodesics of a Kerr black hole with $\bar{a} = 0.5$ as functions of the radius \bar{r} . Their sum gives the corrected precession $\zeta_{(\text{cor})}(U, m, E)^{\hat{z}}/\gamma(U, m)$ with respect to the threading observers, shown as the long dashed curve. Since these are all finite, the corrected precession terms themselves all diverge at the ergosphere boundary.

to the threading observer axes. For the corotating circular geodesics in the Gödel spacetime, only the gravitomagnetic precession is nonzero and has the same value as for the counter-rotating geodesics.

These results agree with those of Rindler and Perlick⁷ and Iyer and Vishveshwara,^{35,36} both of whom use rotating coordinates $t' = t$, $\phi' = \phi - \omega t$ for which the circular orbit has a fixed angular coordinate in order to find the precession angle $\Delta\phi$ of the gyroscope after one loop. This precession angle $\Delta\phi$ and the precession angular velocity $\zeta_{(\text{cor})}(U_{\pm}, m, E)^{\hat{z}}$ are related by a scale factor and an integral over the loop

$$\begin{aligned}\Delta\phi_{\pm} &= \oint \zeta_{(\text{cor})}(U_{\pm}, m, E)^{\hat{z}} d\tau_{U_{\pm}} = \pm \int_0^{2\pi} \zeta_{(\text{cor})}(U_{\pm}, m, E)^{\hat{z}} \frac{d\tau_{U_{\pm}}}{d\phi} d\phi \\ &= \pm [2\pi/\nu(U_{\pm}, m)^{\hat{\phi}}] \gamma(U_{\pm}, m)^{-1} \zeta_{(\text{cor})}(U_{\pm}, m, E)^{\hat{z}},\end{aligned}\quad (6.14)$$

using equation (6.11) and recalling the proper time conversion factor. Comparing this with equation (6.12) and recalling the additional gamma factor in equation (6.1) shows that the contribution to the total precession angle from the corrected space curvature precession equals the threading deficit angle $\Delta(m)$ modulo the sign

$$\Delta\phi_{\pm(\text{sc,cor})} = \pm\Delta(m). \quad (6.15)$$

Of course, with some more formula juggling one can obtain the spin precession for the case of circular orbits with arbitrary acceleration. To express this as a function of the relative velocity and radius, one need only replace $F(U, m)^{\hat{r}}$ in the radial component of the $u = m$ version of Eq. (6.2) by $\gamma(U, m)^{-1} f(U, m)^{\hat{r}}$, where the physical force $f(U, m)^{\hat{r}}$ is itself expressed in terms of those variables by Eq. (4.3). For example, the Thomas precession term has the form

$$\begin{aligned}\zeta_{(\text{thom})}(U, m)^{\hat{z}} &= \nu(U, m)^{\hat{\phi}} [\gamma(U, m) + 1]^{-1} f(U, m)^{\hat{r}} \\ &= \kappa(\phi, m)^{\hat{r}} \nu(U, m)^{\hat{\phi}} [\gamma(U, m) + 1]^{-1} \gamma(U, m)^2 \\ &\quad \times [\nu(U, m)^{\hat{\phi}} - \nu(U_-, m)^{\hat{\phi}}] [\nu(U, m)^{\hat{\phi}} - \nu(U_+, m)^{\hat{\phi}}].\end{aligned}\quad (6.16)$$

Gathering the preliminary expressions for the other precession terms and doing some involved algebra in which Eqs. (4.6) are helpful leads to the following general result for the total precession angular velocity

$$\begin{aligned}\zeta(U, m, E)^{\hat{z}} &= \frac{1}{2} \gamma(U, m)^{-2} (d\mathcal{F}/d\nu) (\nu(U, m)^{\hat{\phi}}; \kappa(\phi, m)^{\hat{\phi}}, \nu(U_-, m)^{\hat{\phi}}, \nu(U_+, m)^{\hat{\phi}}), \\ \zeta_{(\text{cor})}(U, m, E)^{\hat{z}} &= \zeta(U, m, E)^{\hat{z}} + \gamma(U, m) \nu(U, m)^{\hat{\phi}} / \gamma_{\phi\phi}^{1/2},\end{aligned}\quad (6.17)$$

generalizing Eq. (6.10) to the accelerated case for all the spacetimes under consideration.

The precession angular velocity $\zeta(U, m, E)^{\hat{z}}$ thus vanishes at the critical points of the radial physical force function, corresponding to the locking of the spin to the static spherical frame for the extremal force observers. These observers act as

the boundary between the counter-rotating and corotating spin precession orbits relative to the radial direction. Table 8 correlates the sign of this precession with these intervals of relative velocity values in each of the three regions A, B, and C assuming $\nu_- + \nu_+ < 0$. In the limiting Schwarzschild case where region B disappears and $\nu_{(\text{ext})} = 0$, the spin precession $\zeta(U, m, E)^{\hat{z}}$ has the opposite sign compared to the angular velocity in region A and the same sign in region C.

Table 8. Signs of the spin precession for circular orbits of a given angular relative velocity.

	Region A	Region B	Region C
$\zeta(U, m, E)^{\hat{z}} > 0$	$(-1, \nu_{(\text{ext})})$	—	$(\nu_{(\text{ext})}, 1)$
$\zeta(U, m, E)^{\hat{z}} = 0$	$\nu_{(\text{ext})}$	—	$\nu_{(\text{ext})}$
$\zeta(U, m, E)^{\hat{z}} < 0$	$(\nu_{(\text{ext})}, 1)$	$(-1, 1)$	$(-1, \nu_{(\text{ext})})$

Using the properties of the function \mathcal{F} introduced in Eq. (4.7) and the relation (4.6), the gyro spin precession angular velocity with respect to the static spherical frame from its own point of view takes a very simple form analogous to the physical acceleration it experiences

$$\begin{aligned}\zeta(U, m, E)^{\hat{z}} &= -\mathcal{F}(\nu(U, m)^{\hat{\phi}}; H(m)^{\hat{z}}/2, \nu_{(\text{crit})-}(U, m)^{\hat{\phi}}, \nu_{(\text{crit})+}(U, m)^{\hat{\phi}}), \\ a(U)^{\hat{r}} &= \mathcal{F}(\nu(U, m)^{\hat{\phi}}; \kappa(\phi, m)^{\hat{r}}, \nu(U_-, m)^{\hat{\phi}}, \nu(U_+, m)^{\hat{\phi}}).\end{aligned}\quad (6.18)$$

One can then carry over to the spin precession the entire analysis of the extrema of the physical force function $a(U)^{\hat{r}}$. Defining a relative difference velocity by Eq. (4.9) with ν_{\pm} replaced by $\nu_{(\text{crit})\pm}$ leads to $\nu_{(\text{rel}, \text{spin})} = 1/\nu_{(\text{rel})}$ which is in the physical range only in region B where $|\nu_{(\text{rel})}| > 1$, $\nu_{(\text{crit})\pm}$ are complex, and the spin precession is always negative.

Only in this region are the corresponding critical values related to this new relative velocity by Eq. (4.10) real

$$\nu_{(\text{crit}, \text{spin})\pm} = \mathcal{V}_{\pm}(1/\nu_{(\text{rel})}) = \nu_{(\text{rel})} \left[1 \pm \sqrt{1 - 1/\nu_{(\text{rel})}^2} \right]. \quad (6.19)$$

As before only the minus root is in the physical range leading to the spin extremal velocity

$$\nu_{(\text{ext}, \text{spin})} = \nu_{(\text{rel})} \left[1 - \sqrt{1 - 1/\nu_{(\text{rel})}^2} \right] \quad (6.20)$$

at which a maximum negative (but minimum absolute value) spin precession angular velocity occurs with value

$$-\mathcal{F}(\nu_{(\text{ext}, \text{spin})}; H/2, \nu_{(\text{crit})-}, \nu_{(\text{crit})+}) = -\frac{1}{2}H[2 + \gamma_{(\text{rel}, \text{spin})}]/\gamma_{(\text{rel}, \text{spin})}. \quad (6.21)$$

Figure 5(b) illustrates the geometry of the relative observer plane associated with this analysis.

Figure 9 shows both (a) the spin precession $\zeta(U, m, E)^{\hat{z}}$ and (b) the corrected spin precession $\zeta_{(\text{cor})}(U, m, E)^{\hat{z}}$ at the same selected radii as a function of the threading relative velocity for a Kerr black hole with $\bar{a} = 0.5$ outside the ergosphere where the spin precession with respect to the distant stars makes sense. The intersections of these curves with the short dashed curves in Figure 9(b) occur at the velocities of the geodesic orbits, corresponding to Figure 8. The long dashed curves mark the boundaries $r_{(\text{AB})}$, $r_{(\text{BC})}$ between the regions A, B, and C. One can see three families of observers in region A for which the corrected precession vanishes. Upon closer inspection one sees that there is one pair which respectively corotate and counterrotate faster than the pair of timelike circular geodesics and share the same respective observer horizons, and another family near the slicing observers which has the ergosphere as its horizon.

Working instead with the coordinate angular velocity, de Felice³¹ has shown (following from a comparison of Refs. 31 and [28], see also Ref. 24) and implied the fact that the corotating Fermi-Walker spin precession vanishes exactly at the two critical points of the radial force function, and is positive between them and negative outside. In the approach of Iyer and Vishveshwara³⁶ for stationary axially symmetric spacetimes, specialized to their equatorial plane case $\tau_2 = 0 = \mathcal{A}_{(2)}$, the precession angular velocity $\zeta(U, m, E)^{\hat{z}}$ is just the sign-reversal of the first Serret-Frenet torsion τ_1 and the acceleration $a(U)^{\hat{r}}$ of the test particle (physical force) is the Serret-Frenet curvature κ . For the equatorial plane case their Eq. (50) in their notation reduces to

$$\begin{aligned} \tau_1 &= \frac{1}{2}\mathcal{A}/\sqrt{\Delta_3}\partial_\omega\kappa = -\frac{1}{2}[M\Gamma(U, m)^2\gamma_{\phi\phi}^{1/2}]^{-1}\partial_\zeta a(U)^{\hat{r}} \\ &= -\frac{1}{2}\gamma(U, m)^{-2}\partial_\nu\mathcal{F} = -\zeta(U, m, E)^{\hat{z}}. \end{aligned} \quad (6.22)$$

This first torsion is called the Fermi drag by de Felice. In the case of general motion along a Killing trajectory in a stationary axially symmetric spacetime, one can show that the gyro spin precession angular velocity (Eq. (20) of Ref. 36) relative to the Frenet-Serret frame E_a^α is just

$$-\omega(U)_{(\text{FS})}^\alpha = P(U, u)^\alpha{}_\beta \zeta(U, u, E)^\beta. \quad (6.23)$$

7. Sagnac effect and synchronization defect

The Sagnac effect^{45–48} and its timelike analog, both of which in turn are connected to the synchronization defect,⁴⁹ refer to the asymmetry in the arrival times of a pair of oppositely rotating timelike geodesic or null circular orbits at a given radius as seen by a given rotating observer. If (ζ_1, ζ_2) is the ordered pair of coordinate angular velocities of such a pair (either (ζ_-, ζ_+) or $(\dot{\phi}_-, \dot{\phi}_+)$), and ζ is the angular velocity of a rotating observer with 4-velocity U distinct from this pair, one easily finds that the difference and average of the coordinate arrival times after one complete revolution with respect to this observer are

$$\Delta t = \mathcal{S}(\zeta; \zeta_1, \zeta_2) = t_2 - t_1 = 2\pi [1/(\zeta_2 - \zeta) - 1/(\zeta - \zeta_1)]$$

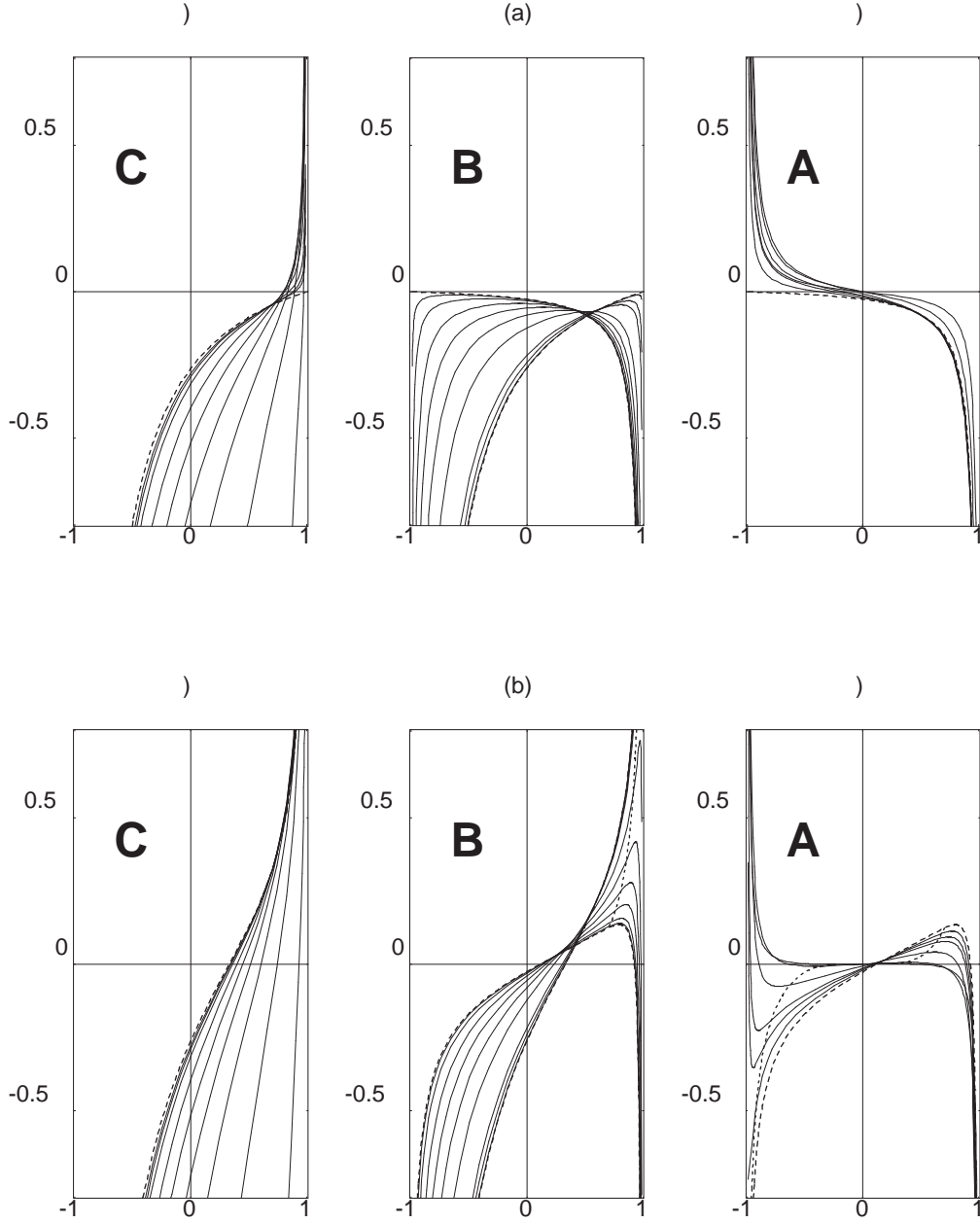


Fig. 9. ζ versus ν : plots of (a) the precession angular velocity $\zeta(U, m, E)^{\hat{z}}$ and (b) the corrected precession angular velocity $\zeta_{(\text{cor})}(U, m, E)^{\hat{z}}$ of the spin of a gyroscope versus the orbital physical angular velocity for selected radii for equatorial circular orbits of a Kerr black hole with $a = 0.5$.

$$\begin{aligned}
 &= -4\pi[\zeta - (\zeta_1 + \zeta_2)/2]/[(\zeta - \zeta_1)(\zeta - \zeta_2)] , \\
 t_{(\text{avg})} &= (t_1 + t_2)/2 = 2\pi [1/(\zeta_2 - \zeta) + 1/(\zeta - \zeta_1)] \\
 &= \pi[\zeta_1 - \zeta_2]/[(\zeta - \zeta_1)(\zeta - \zeta_2)] , \tag{7.1}
 \end{aligned}$$

the ratio of which gives the relative difference in the coordinate arrival times

$$\Delta t/t_{(\text{avg})} = 4[\zeta - (\zeta_1 + \zeta_2)/2]/[(\zeta_1 - \zeta_2)/2] . \tag{7.2}$$

For the pair of oppositely rotating timelike geodesics one has

$$\Delta t_{(\text{geo})}(U) = \mathcal{S}(\zeta; \dot{\phi}_-, \dot{\phi}_+) = -4\pi[\zeta - \zeta_{(\text{gmp})}]/[(\zeta - \dot{\phi}_-)(\zeta - \dot{\phi}_+)] , \tag{7.3}$$

while for the pair of oppositely rotating null orbits one has

$$\Delta t_{(\text{null})}(U) = \mathcal{S}(\zeta; \zeta_-, \zeta_+) = -4\pi[\zeta - \zeta_{(\text{nmp})}]/[(\zeta - \zeta_-)(\zeta - \zeta_+)] , \tag{7.4}$$

recalling that $\zeta_{(\text{nmp})} = \zeta_{(\text{sl})}$. Each of these may be evaluated for the slicing, threading, and extremal force observers, when the three orbits are distinct for a given application. Note that the null arrival time difference is proportional to the angular momentum (2.11) of U .

The Sagnac time difference and its timelike geodesic analog are given when the observer is taken to be the threading observer

$$\begin{aligned}
 \Delta t_{(\text{null})}(m) &= \mathcal{S}(0; \zeta_-, \zeta_+) = 4\pi\zeta_{(\text{nmp})}/(\zeta_- \zeta_+) \\
 &= 4\pi(\zeta_-^{-1} + \zeta_+^{-1})/2 = 4\pi M_\phi , \\
 \Delta t_{(\text{geo})}(m) &= \mathcal{S}(0; \dot{\phi}_-, \dot{\phi}_+) = 4\pi\zeta_{(\text{gmp})}/(\dot{\phi}_- \dot{\phi}_+) \\
 &= 4\pi(\dot{\phi}_-^{-1} + \dot{\phi}_+^{-1})/2 = 4\pi a \quad [\text{Kerr}] . \tag{7.5}
 \end{aligned}$$

The null difference is positive/negative when the threading observers corotate/-counter-rotate with respect to the slicing observers ($\text{sgn } \Delta t_{(\text{null})} = \text{sgn } N^\phi = \text{sgn } M_\phi$). The geodesic difference is positive assuming an upward gravitomagnetic field ($\text{sgn } \Delta t_{(\text{geo})} = \text{sgn } H^{\hat{z}}$), with the counterrotating geodesic returning first to the threading observer ($t_2 < t_1$, where 2 labels the corotating geodesic). The geodesic formula is not valid for Gödel since the threading observer is itself geodesic, nor for Minkowski which only has one geodesic.

The synchronization defect is just half the Sagnac time difference and indicates the change in coordinate time which occurs during one corotating spatial loop (ϕ coordinate line in spacetime)

$$\Delta t_{(\text{SD})}(m) = \int_0^{2\pi} M_\phi d\phi = 2\pi M_\phi = \Delta t_{(\text{null})}(m)/2 . \tag{7.6}$$

The analogous coordinate time difference for the geodesic case in the Kerr spacetime

$$2\pi/\bar{\zeta}_{(\text{car})} = \Delta t_{(\text{geo})}(m)/2 = 2\pi a \tag{7.7}$$

corresponds exactly to one threading loop of a circular curve which is spatial with respect to a Carter observer ($\zeta_{(\text{car})} = a/(a^2 + r^2)$, so $\bar{\zeta}_{(\text{car})} = 1/a$ by Eq. (2.12)), connecting the average-time-of-return point on the threading observer world line with either return point on the same world line.

Figure 10 shows the relationship between the arrival times of oppositely rotating circular geodesic and null orbits and the Sagnac effect and its timelike geodesic analog in region A. This is illustrated for the case in which the shift is negative as in the Kerr spacetime, i.e., the threading observers counter-rotate with respect to the slicing observers, so the corotating null orbit returns first to the threading observer from which it originated. Independent of the sign of the shift but assuming that the gravitomagnetic field is upward, the geodesic meeting point observer counter-rotates with respect to both the slicing and threading observers, and the extremal force observers counter-rotate in turn with respect to the geodesic meeting point observers. Even though the extremal force observers see the oppositely rotating pair of geodesics moving with the same speed, the counter-rotating geodesic arrives after the corotating one as shown.

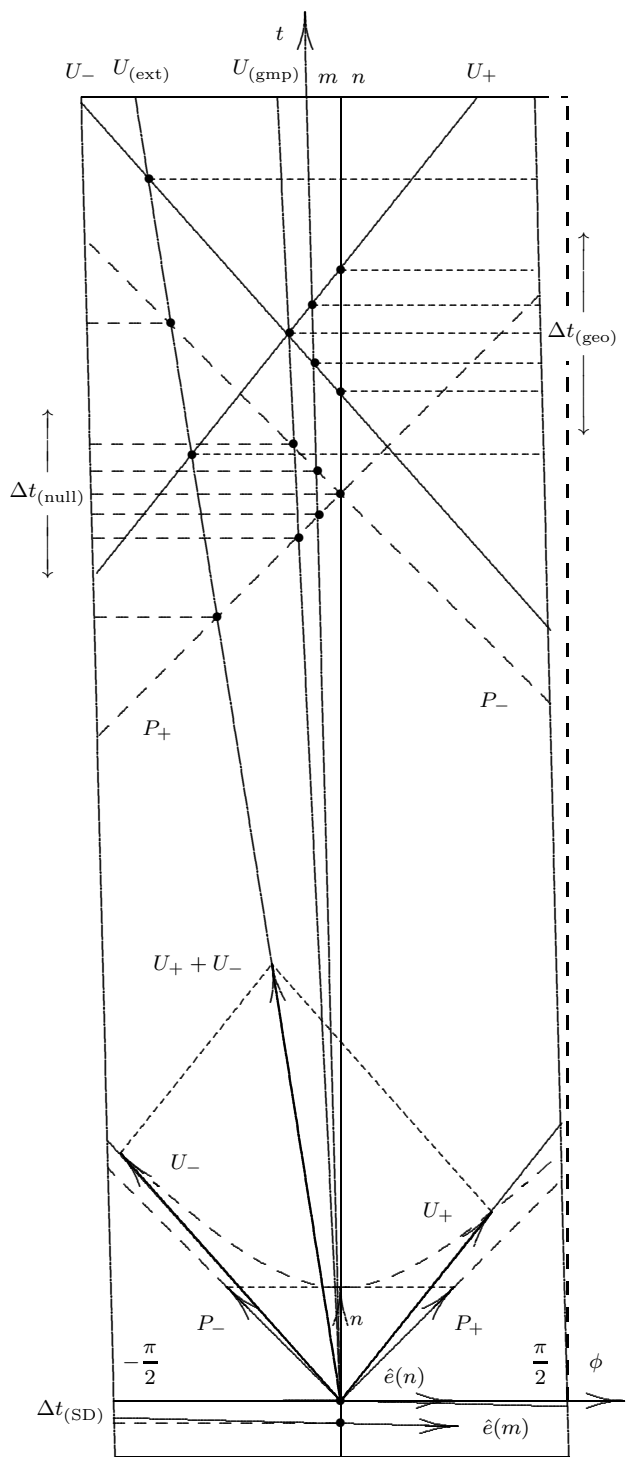
The horizontal unit vector $\hat{e}(n)$ in Figure 10 is along the slicing relative velocity direction tangent to the ϕ coordinate line (constant t). The horizontal short dashed line connecting P_{\pm} contains all the (horizontal) slicing relative velocities. The unit vector $\hat{e}(m)$ is along the threading relative velocity direction and indicates the threading local rest space angular direction. Extending this forward around one loop of the cylinder leads to the change in the coordinate time equal to the synchronization defect.

One can express the threading observer synchronization defect, Sagnac effect, and timelike geodesic generalization of it using a single formula involving the physical fields. The 1-form

$$\begin{aligned} \gamma(U, m)^{-1} \bar{U}_{\alpha} dx^{\alpha} &= [m_{\alpha} + 1/\nu(U, m)^{\hat{\phi}} e(m)_{\alpha}] dx^{\alpha} \\ &= -M(dt - M_{\phi} d\phi) + \gamma_{\phi\phi}^{1/2}/\nu(U, m)^{\hat{\phi}} d\phi \end{aligned} \quad (7.8)$$

orthogonal to the 4-velocity U^{α} restricts to zero along the world line, so the observer

Fig. 10. The conformal diagram of the front half $[-\pi/2, \pi/2] \times R$ of the flattened t - ϕ coordinate cylinder for a fixed r in region A, showing the null and geodesic time differences for corotating and counter-rotating orbits for the various observer families. The vertical axis is along the (null meeting point) slicing observers (n), the time coordinate axis is along the threading observer direction (m), and the horizontal axis is along the ϕ coordinate direction (constant t). The diagram illustrates the case in which the slicing observers corotate with respect to the threading observers as in Kerr so that the time lines tilt to the left. The relative observer plane tangent space (region A case) is superimposed on the cylinder together with the corresponding world lines emanating from a given single initial point. The slicing, threading, geodesic meeting point, and extremal force observer 4-velocities and world lines are shown, together with the null 4-momenta $P_{\pm}^{\alpha} = n^{\alpha} \pm \hat{e}(n)^{\alpha}$ of the two oppositely rotating null orbits. The synchronization defect is shown at the bottom of the figure corresponding to one loop of a threading purely spatial curve with unit tangent $\hat{e}(m)^{\alpha}$.



proper time arrival time is

$$\begin{aligned}\tau(m) &= Mt(m) = [\text{sgn } \nu(U, m)^{\hat{\phi}}] \int_0^{2\pi} [MM_\phi + \gamma_{\phi\phi}^{1/2}/\nu(U, m)^{\hat{\phi}}] d\phi \\ &= 2\pi M/|\zeta| .\end{aligned}\tag{7.9}$$

Thus difference in arrival times of two oppositely directed world lines is then

$$\Delta\tau(m) = M[t_2(m) - t_1(m)] = 2\pi \left[MM_\phi + \gamma_{\phi\phi}^{1/2} [1/\nu(U_1, m)^{\hat{\phi}} + 1/\nu(U_2, m)^{\hat{\phi}}] \right] .\tag{7.10}$$

For the oppositely directed null orbits ($\nu(P, m)^\phi = \pm 1$), this just gives

$$\Delta\tau_{(\text{null})}(m) = 4\pi MM_\phi = 4\pi p_\phi(m) ,\tag{7.11}$$

namely the conserved angular momentum of the threading observers. For the oppositely directed timelike geodesic orbits this just gives

$$\Delta\tau_{(\text{geo})}(m) = 4\pi p_\phi(m) - C(m)H(m)^{\hat{z}}/g(m)^{\hat{r}} ,\tag{7.12}$$

where $C(m) = 2\pi\gamma_{\phi\phi}^{1/2}$ is the threading circumference of a ϕ coordinate circle, using Eq. (4.6) to re-express the quotient of the sum and product of the geodesic relative velocities. For the limit $\nu(U_i, m) \rightarrow \pm\infty$ in which the trajectories become spatial curves with respect to m , this gives twice the synchronization defect (defined to be the change in time around one such loop, not two) which has the same value as the proper time Sagnac effect

$$\Delta\tau_{(\text{SD})}(m) = \frac{1}{2}\Delta\tau_{(\text{null})}(m) .\tag{7.13}$$

These same considerations should apply to any stationary family of observers, once they are expressed in terms of the threading potentials and fields associated with the family. For the slicing observers, for example, both the angular momentum and the threading gravitomagnetic field vanish so the Sagnac and synchronization defects vanish.

Similarly the slicing point of view expression for the proper time geodesic effect has an analogous formula with the substitutions $H(m)^{\hat{z}} \rightarrow -2\theta(n)_{\hat{\phi}\hat{r}}$, $C(m) \rightarrow C(n) = 2\pi g_{\phi\phi}^{1/2}$

$$\Delta\tau_{(\text{geo})}(n) = 0 + 2C(n)\theta(n)^{\hat{\phi}\hat{r}}/g(n)^{\hat{r}} ,\tag{7.14}$$

since the slicing angular momentum vanishes.

8. Concluding Remarks

Test particle behavior is one of the most important tools in interpreting the local spacetime structure of a given spacetime, whether it is a nice exact solution with symmetry which may be worked with analytically or an approximate solution with no symmetry derived with very complicated mathematical machinery. The three

familiar spacetimes analyzed here in terms of natural test observer families each have a rich and interesting geometry that weaves together in slightly different ways the various effects that their gravitational fields have on the motion and spin of test particles.

By adopting a general approach to the test observer splitting and the geometry they use to interpret their measurements, many diverse issues heretofore described in widely differing languages are brought together in a single discussion based on familiar observer-defined quantities. Instead of vague references to centrifugal and Coriolis forces that motivate the interpretation of fields in linearized approximations to general relativity or the somewhat obscure formal representations of such forces in the fully nonlinear theory, this general approach gives a clear and precise representation of the many ways these concepts can manifest themselves in the arena of Einstein's theory. By analyzing these three familiar spacetimes in this approach, and showing the power that it has in interpreting physical aspects of their geometry and showing the wider applicability of the analysis to allow comparisons among them, we hope to encourage others to consider its use when appropriate.

Acknowledgements

We thank Remo Ruffini of the International Center for Relativistic Astrophysics at the University of Rome and Francis Everitt of the Gravity Probe B Relativity Mission group at Stanford University for their support and encouragement of this work.

A. Embedding cross-section diagrams

For the 2-dimensional metrics in polar-like coordinates $\{r, \phi\}$ under consideration

$$h_{rr}dr^2 + h_{\phi\phi}d\phi^2 = h_{RR}dR^2 + R^2d\phi^2, \quad (\text{A.1})$$

where the components depend only on the radial coordinate, the embedding into E_3 or M_3 with cylindrical coordinates $\{R, \phi, Z\}$ can be accomplished in two steps. First one inverts the transformation from the radial coordinate r to the radial circumferential arclength coordinate $R = h_{\phi\phi}^{1/2}r$, for which the circumference of a radial coordinate circle has the usual expression $2\pi R$. Then one performs an integral to get the curve in the R - Z half plane which is the constant ϕ cross-section of the embedding surface. It is convenient for graphing purposes to introduce the rescaled variables $\bar{R} = R/\mathcal{R}$ and $\bar{Z} = Z/\mathcal{R}$ analogous to $\bar{r} = r/\mathcal{R}$, where \mathcal{R} is the length scale of Table II. The case $h_{RR} = 1$ corresponds to the flat case of E_2 in polar coordinates. When $h_{RR} > 1$, one next identifies the result with the flat cylindrical coordinate metric on E_3 restricted to the surface $Z = Z(R)$

$$dR^2 + R^2d\phi^2 + dZ(R)^2 = [1 + (dZ(R)/dR)^2]dR^2 + R^2d\phi^2. \quad (\text{A.2})$$

If instead $h_{RR} < 1$, one identifies the result with the flat cylindrical coordinate metric on M_3 restricted to the surface $Z = Z(R)$, where Z is now a timelike

coordinate

$$dR^2 + R^2 d\phi^2 - dZ(R)^2 = [1 - (dZ(R)/dR)^2]dR^2 + R^2 d\phi^2 . \quad (\text{A.3})$$

In both cases this gives a first order differential equation for $Z(R)$ with an integral solution as in the Schwarzschild case³⁸

$$1 \pm (dZ(R)/dR)^2 = h_{RR} = h_{rr}(dr/dR)^2 , \quad (\text{A.4})$$

or equivalently

$$\begin{aligned} |dZ(R)/dR| &= \sqrt{\pm(h_{RR} - 1)} , \\ |Z(R) - Z_0| &= \int_{R_0}^R \sqrt{\pm(h_{RR} - 1)} dR , \end{aligned} \quad (\text{A.5})$$

where the plus/minus sign corresponds to the embedding in E_3/M_3 . Dropping the absolute value sign, Z may be chosen initially to increase with R , but a negative derivative may later be required if the embedding turns back towards the Z -axis as Z increases.

In general it is not possible to express the argument of the square root explicitly as a function of R but one can make a parametric plot of $Z(r)$ and $R(r)$ using

$$\begin{aligned} |dZ(r)/dr| &= \sqrt{\pm[h_{rr} - (dR(r)/dr)^2]} , \\ R(r) &= \sqrt{h_{\phi\phi}} , \end{aligned} \quad (\text{A.6})$$

which has the integral solution

$$|Z(r) - Z_0| = \int_{r_0}^r \sqrt{\pm[h_{rr} - (dR(r)/dr)^2]} dr . \quad (\text{A.7})$$

This may be numerically integrated if necessary.

For cases with a regular origin $R \rightarrow 0$ as $r \rightarrow 0$, the initial conditions $Z_0 = 0$ and $r_0 = 0$ puts the origin of the $\{r, \phi\}$ coordinate system at the origin of the embedding space. In other cases, one may start at a physically interesting value of r for r_0 , which then determines R , and choose Z_0 conveniently.

Once the curve in the R - Z plane is obtained either analytically or numerically, the full surface is obtained by revolving it around the Z axis. Introducing the Lie relative radius of curvature from [BCJ1] for this context

$$\rho(\phi, u) = |\kappa(\phi, u)^{\hat{r}}|^{-1} = |-(\ln R)_{,r}/h_{rr}^{1/2}|^{-1} \quad (\text{A.8})$$

leads to the result $h_{RR}^{1/2} = \rho(\phi, u)/R$ and

$$|dZ(R)/dR| = \sqrt{\pm[\rho(\phi, u)^2/R^2 - 1]} = \sqrt{\pm[\rho(\phi, u)^2 - R^2]}/R . \quad (\text{A.9})$$

The ratio $\rho(\phi, u)/R$ is identically 1 for a flat space, greater than 1 for a Euclidean embedding, and less than 1 for a Minkowski embedding. In the latter cases, if

this ratio passes through 1 at some radius, the tangent to the R - Z cross-section is horizontal and the embedding space signature switches sign. This tangent line is instead vertical when $|dZ(R)/dR| \rightarrow \infty$, which occurs when $\rho(\phi, u) \rightarrow \infty$ at a Lie relatively straight circle. On either side of the radius $r_{(\text{ss})}$ at which the signature switches sign, the choice of sign for the derivative $dZ(r)/dr$ is free. This sign will be always be chosen to be positive to join the two embedding spaces on either side of a half plane, in which case

$$\text{sgn}(\kappa(\phi, u)^{\hat{r}}) = -\text{sgn}(dZ/dR) . \quad (\text{A.10})$$

Embedding diagrams for which the signature changes have been used by Smarr⁵⁰ in studying the 2-surface cross-section of the horizon of a charged Kerr black hole.

When the tangent to the embedding cross-section is not vertical, one can introduce the tangent cone obtained by revolving the tangent line at a point $(R, Z(R))$ on the cross-section. The relation (A.9) then shows that $\rho(\phi, u)$ must be identified with the distance of the tangent line point of contact from the vertex of the cone calculated in the embedding space geometry, thus giving a nice geometrical interpretation to the Lie relative radius of curvature. For the E_3 case, the defect angle of the cone is easily found to have the positive value

$$\Delta = 2\pi[1 - R/\rho(\phi, u)] , \quad (\text{A.11})$$

which in the usual case in which $\text{sgn}(\kappa(\phi, m)^{\hat{r}}) < 0$ determines the space curvature contribution to the precession angle of the spin of a gyroscope following the circular orbit after one revolution modulo the sign, as discussed by Thorne.⁵¹ The same formula holds for the spacelike cones in M_3 , where the defect angle is instead negative. Note that in approaching a relatively straight trajectory (vertical tangent in the R - Z cross-section) this defect angle approaches 2π , while in approaching a horizontal tangent in the R - Z cross-section the angle approaches the flat value 0.

The Gaussian curvature of this surface is easily evaluated from standard formulas to be

$$K = -(Rh_{rr}^{-1/2})^{-1}(R_{,r}/h_{rr}^{-1/2})_{,r} = -R^{-1}R_{,\hat{r}\hat{r}} . \quad (\text{A.12})$$

For the rotating Minkowski slicing and the Gödel threading cases where $h_{rr} = 1$, this reduces to $K = -R^{-1}R_{,rr}$. This may also be rewritten as

$$K = \text{sgn}(\kappa(\phi, u)^{\hat{r}}) R^{-1}[R/\rho(\phi, u)]_{,\hat{r}} . \quad (\text{A.13})$$

Thus the sign of the Gaussian curvature depends on the signs of the radial relative centripetal acceleration (sign of $-R_{,r}$) and of the radial derivative of the ratio $R/\rho(\phi, u)$. It is also straightforward to show that

$$\text{sgn}(K) = \mp \text{sgn}(d^2 R/dZ^2) , \quad (\text{A.14})$$

which implies that when the cross-section curve is concave away/toward the Z -axis in E_3 , the Gaussian curvature is negative/positive, and vice versa in M_3 .

A.1. Rotating Minkowski spacetime

The spatial geometry in the slicing point of view is flat, so the usual Euclidean geometry applies and the Lie signed relative curvature of the ϕ coordinate lines is just the reciprocal of the radial coordinate r .

The r - ϕ surface in the threading point of view is instead an inhomogeneous surface of revolution of negative Gaussian curvature $-3\gamma^4/\mathcal{R}^2$ which starts at the value $-3/\mathcal{R}^2$ at the origin and as r increases it decreases to $-\infty$ at the observer horizon at the value $\bar{r}_{(h)} = 1$. The embedding is in M_3 and the singularity at the observer horizon occurs at $R \rightarrow \infty$. Figure 11(a) shows the constant ϕ cross-section of this surface, with the horizontal and vertical axes showing the rescaled variables $\bar{\mathcal{R}}$ and \bar{Z} respectively.

The threading case

Since $dR/dr = \gamma^3$ is always positive, then $h_{RR} = \gamma^{-6} < 1$ and the embedding occurs in M_3 with a regular origin and a single sign for $dZ(R)/dR$ which may be taken to be positive. The relationship $\bar{R} = \gamma\bar{r}$ (with $\gamma = (1 - \bar{r}^2)^{-1/2}$) inverts to $\bar{r} = \gamma^{-1}\bar{R}$ (with $\gamma = (1 + \bar{R}^2)^{1/2}$). Dropping the absolute value signs in the embedding equation (A.5) and choosing $\bar{Z}_0 = 0$ leads to

$$\bar{Z}(\bar{R}) = \int_0^{\bar{R}} \sqrt{1 - (1 + x^2)^{-3}} dx . \quad (\text{A.15})$$

The change of variable $w = 2 \ln \gamma = \ln(1 + \bar{R}^2) = -\ln(1 - \bar{r}^2)$ leads to

$$\bar{Z}(w) = \frac{1}{2} \int_0^w \sqrt{1 + 2 \cosh y} dy , \quad (\text{A.16})$$

which in turn suggests the further change of variable $u = \sinh(w/2) = (\gamma - \gamma^{-1})/2$ and

$$\begin{aligned} \bar{Z}(u) &= 2 \int_0^u \sqrt{(3/4 + v^2)/(1 + v^2)} dv \\ &= -\frac{3}{2}[F(\alpha, 1/2) - F(\pi/2, 1/2)] + 2[E(\alpha, 1/2) - E(\pi/2, 1/2)] \\ &\quad + 2u\sqrt{(1 + u^2)/(3/4 + u^2)} , \end{aligned} \quad (\text{A.17})$$

where $\alpha = \arctan(1/u)$ by a slightly corrected version of formula 3.169.2 on p.276 of Gradshteyn and Ryzhik,⁵⁴ and $F(\varphi, k)$ and $E(\varphi, k)$ are elliptic integrals of the first and second kind in their notation. (When using MAPLE V and Mathematica respectively, the correspondence is $E(\varphi, k) = \text{LegendreE}(\sin \varphi, k) = \text{EllipticE}(\varphi, k^2)$.)

A.2. Gödel spacetime

Figure 11 shows the constant ϕ cross-section of the r - ϕ surface with the horizontal and vertical axes showing the rescaled variables $\bar{\mathcal{R}}$ and \bar{Z} respectively in the (b) threading and (c) slicing points of view.

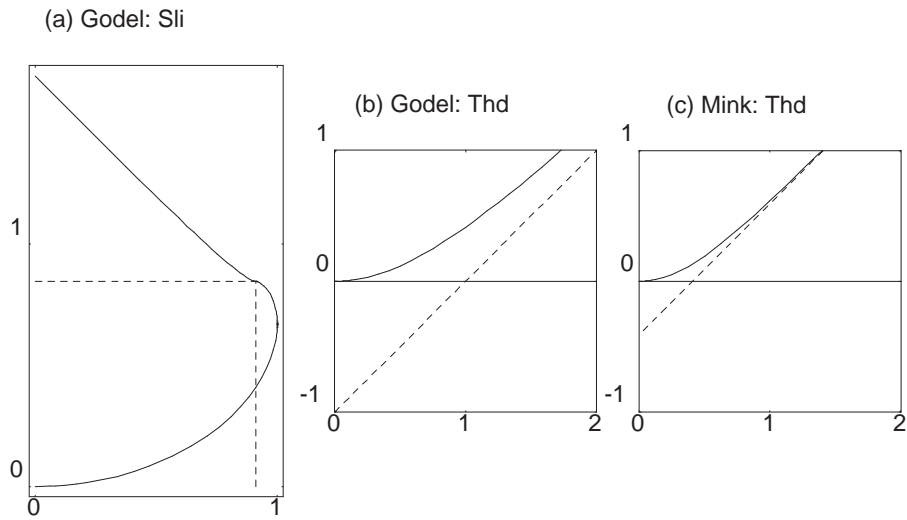


Fig. 11. \bar{Z} versus \bar{R} : embedding cross-section diagram for the r - ϕ surfaces in the threading point of view for the Gödel (a) slicing and (b) threading points of view and (c) the rotating Minkowski threading point of view. In the latter two cases the asymptotic null lines in the M_3 embedding are shown with respective intercepts $\bar{Z} \approx -0.567\bar{r}_{(\text{hor})}$ and $\bar{Z} \approx -0.406\bar{r}_{(\text{hor})}$ which are comparable fractions of the horizon scale, but which appear much different since units of vorticity rather than curvature are used in the graph. In the first case starting at the origin with a Euclidean embedding, the embedding surface moves away from the vertical axis and then turns back at the radius of the single relatively straight circle, next switching signature and finally asymptotically approaching the vertical axis again at the observer horizon along an asymptotic null cone.

In the threading point of view the spatial metric of the r - ϕ surface is in one of the standard forms for a constant negative-curvature geometry ($K = -1/\mathcal{R}^2$) and is easily embedded in M_3 as a spacelike pseudosphere of radius \mathcal{R} . The circumference R of the circles of constant radial coordinate increases without bound but the magnitude of the Lie signed relative curvature approaches a lower limit corresponding to a maximum Lie relative radius of curvature of magnitude \mathcal{R} , a consequence of the negative curvature geometry.

In the slicing point of view where r is a radial arclength coordinate this surface has positive Gaussian curvature $K = (2\mathcal{R}^2)^{-1}(1+2s^2-2s^4)/(1-s^2)^2$ which increases from the value $1/(2\mathcal{R}^2)$ at the origin to infinity at the observer horizon. R begins to decrease with increasing r after reaching the Lie relatively straight circle at the value $\bar{r}_{(\text{rs})} = 2\text{arcsinh}(2^{-1/2}) \approx 1.317$ ($\bar{R}_{(\text{rs})} = 1$) where the Lie signed relative curvature changes sign and the embedding turns back toward the Z -axis. Beyond that the Lie relative centripetal acceleration points outward, i.e., towards larger r values (but smaller R values) as occurs for the optical relative centripetal acceleration close to the horizon in the Schwarzschild spacetime as shown by Abramowicz.^{11–13} The embedding then switches from E_3 to M_3 at the value $\bar{r}_{(\text{ss})} = 2\text{arcsinh}(2^{-1/4}) \approx 1.529$ ($\bar{R}_{(\text{ss})} = \sqrt{2\sqrt{2}-2} \approx 0.910$, $\bar{Z}_{(\text{ss})} \approx 0.847$). Finally the embedding surface returns to the Z -axis ($R = 0$) at the value $\bar{r}_{(\text{h})} = 2\text{arcsinh}(1) \approx 1.763$ ($\bar{Z} = 2\bar{Z}_{(\text{h})}$) corresponding to the observer horizon, where the embedding is singular.

The threading case

Here the standard embedding with $r = 0$ at the origin of M_3 is a pseudosphere of radius \mathcal{R}

$$Z = -\mathcal{R} + \sqrt{R^2 + \mathcal{R}^2} . \quad (\text{A.18})$$

The slicing case

The origin $r = 0$ is again regular, so $Z_0 = 0$ is appropriate, and one may drop the absolute value signs initially in the explicit embedding equation (A.5). Since $dR/dr = c(1-2s^2)/\sqrt{1-s^2}$ changes sign as r increases, this embedding turns back toward the Z -axis, after which dR/dr passes through the value 1 where the embedding switches from E_3 to M_3 . Attempting to invert the relationship $\bar{R}(u) = 2\sqrt{u(1-u)} = 2s\sqrt{1-s^2}$ by solving a quadratic equation for $u = s^2$

$$u = \begin{cases} \frac{1}{2} \left(1 - \sqrt{1 - \bar{R}^2} \right) \in [0, 1/2] , \\ \frac{1}{2} \left(1 + \sqrt{1 - \bar{R}^2} \right) \in [1/2, 1] , \end{cases} \quad (\text{A.19})$$

in terms of which ($\bar{r} = 2\text{arcsinh}(\sqrt{u})$). However, \bar{R} is a doublevalued function of \bar{r} or u , so the latter variables are more appropriate to use. The integral

$$\bar{Z} = \int_0^r 2s\sqrt{(1/2 - s^4)/(1 - s^2)} dr$$

$$= \int_0^u 2\sqrt{(1/2 - v^2)/(1 - v^2)} dv \quad (\text{A.20})$$

can be integrated in terms of elliptic integrals depending on the range of u .

• **Embedding in E_3 .** Starting at the regular origin with $u \in [0, \frac{1}{\sqrt{2}}]$ this evaluates to

$$\bar{Z} = 2E\left(\alpha, 1/\sqrt{2}\right) - F\left(\alpha, 1/\sqrt{2}\right), \quad (\text{A.21})$$

where $\alpha = \arcsin(\sqrt{2}u)$, by formula (3.169.9) on p.276 of Gradshteyn and Ryzhik.⁵⁴ Note that the endpoint value $u = 1/\sqrt{2}$ at the signature change corresponds to $\alpha = \pi/2$, while the relatively straight circle at $u = 1/2$ corresponds to $\alpha = \pi/4$. Let $\bar{Z}_{(\text{ss})} = 2E(\pi/2, 1/\sqrt{2}) - F(\pi/2, 1/\sqrt{2}) \approx 0.847$.

• **Embedding in M_3 .** The new initial condition at $u = 1/\sqrt{2}$ for $u \in [1/\sqrt{2}, 1]$ with the change in sign of the square root argument leads to

$$\bar{Z} - \bar{Z}_{(\text{ss})} = 2E(\beta, 1/\sqrt{2}) - F(\beta, 1/\sqrt{2}) - 2\sqrt{(u^2 - 1/2)(1 - u^2)}/u, \quad (\text{A.22})$$

where $\beta = \arcsin(\sqrt{2u^2 - 1}/u)$, by formula (3.169.11) on p.277 of Gradshteyn and Ryzhik.⁵⁴ The observer horizon then occurs as the limiting point where $u = 1$, $\bar{R} = 0$ and $\beta = \pi/2$, so that $\bar{Z} = 2\bar{Z}_{(\text{ss})}$.

A.3. The Kerr spacetime

The Kerr case can only be handled analytically in the limit of the Schwarzschild spacetime. The embedding geometry of the r - ϕ equatorial plane in the Schwarzschild spacetime is well known to be a parabola of revolution in E_3 with its vertex at the observer horizon which occurs at the relatively straight circle (“throat”).³⁸ The integral (A.7) leads to

$$\bar{Z}(\bar{r}) = \int_2^{\bar{r}} \sqrt{2/(u - 2)} du = 2\sqrt{2}(\bar{r} - 2)^{1/2}, \quad (\text{A.23})$$

with $\bar{Z}_0 = 0$ and $\bar{r}_0 = 2$ while $\bar{R} = \bar{r}$, explicitly confirming the parabolic embedding cross-section.

The Kerr equatorial plane must be studied numerically in both points of view since inverting the relationship between r and the circumferential coordinate R or performing the integral (A.7) cannot be done analytically. The slicing embedding diagrams have been given by Sharp⁵² while a useful discussion of the general problem has been given by Romano and Price.⁵³

For the slicing point of view the plus sign is always valid and the embedding occurs in E_3 . The initial conditions are taken to be $\bar{Z}_0 = 0$ and $\bar{r}_0 = \bar{r}_{(\text{h})} = 1 + \sqrt{1 - \bar{a}^2} \in [1, 2]$, leading to $\bar{R}(r_{(\text{h})}) = 2$. Note that $\bar{R}^2 = \bar{r}^2 + \bar{a}^2 + 2\bar{a}^2/\bar{r}$ implies $d\bar{R}/d\bar{r} = (\bar{r}^3 - \bar{a}^2)/(\bar{r}^2\bar{R}) > 0$, which is positive and finite for the physical ranges $0 \leq \bar{a} \leq 1$ and $\bar{r} \geq \bar{r}_{(\text{h})}$. Since $\Delta = 0$ at $r = r_{(\text{h})}$, then $h_{rr} \rightarrow \infty$ as $r \rightarrow r_{(\text{h})}^+$, so

that also $dZ/dR = [dZ(r)/dr] / [dR(r)/dr] \rightarrow \infty$. Thus all the slicing embedding cross-sections start out at $\bar{R} = 2, \bar{Z} = 0$ in the R - Z plane with a vertical tangent as in the Schwarzschild case where that point is the vertex of a parabola.

For the threading point of view the integrand of (A.7) switches sign, while as $\bar{r} \rightarrow \bar{r}_{(\text{erg})}^+ = 2^+, \bar{R} \rightarrow \infty$, so the observer horizon is pushed out to infinity in M_3 as in the Minkowski threading case. Therefore initial conditions are taken to be $\bar{Z}_0 = 0$ and \bar{r}_0 is chosen to be the single real zero of the integrand which occurs for the physical ranges $0 \leq \bar{a} \leq 1, \bar{r} \geq 2$, equivalent to

$$2\bar{r}^2(\bar{r} - 2)^3 + \bar{a}^2[2\bar{r}(\bar{r} - 2)^2 - \bar{a}^2] = 0. \quad (\text{A.24})$$

As shown in Figure 4, these roots lie in the interval $[2, 2.344]$ (approximately) with the endpoint values respectively corresponding to $\bar{a} = 0$ and $\bar{a} = 1$. The example $\bar{a} = 0.5$ has $\bar{r}_{(\text{ss})} \approx 2.157$.

For $\bar{r} > \bar{r}_0$ the plus sign is relevant and the embedding is in E_3 , while for $\bar{r} < \bar{r}_0$ the minus sign is relevant and the embedding is in M_3 . Thus the R -axis is taken to be the signature change line for all values of a , with E_3 above and M_3 below. One also finds that $dR(r)/dr = 0$ at the single real solution of $\bar{r}(\bar{r} - 2)^2 - \bar{a}^2 = 0$ for the allowed values of \bar{r} and \bar{a} , leading to a vertical tangent in the R - Z plane at the Lie relatively straight circle, where the embedding cross-section turns away from the Z -axis.

The Gaussian curvature for both the threading and slicing cases is negative

$$\begin{aligned} \mathcal{M}^2 K_{(\text{th})} &= -\frac{[\bar{r}(\bar{r} - 2)^2 + 3\bar{a}^2(\bar{r} - 1)]}{\bar{r}^4(\bar{r} - 2)^2}, \\ \mathcal{M}^2 K_{(\text{sl})} &= -\frac{(\bar{r}^7 + 5\bar{a}^2\bar{r}^5 - 11\bar{a}^2\bar{r}^4 + 7\bar{a}^4\bar{r}^3 - 2\bar{a}^4\bar{r}^2 + \bar{a}^4(3\bar{a}^2 - 8)\bar{r} - 7\bar{a}^6)}{\bar{r}^4[\bar{r}(\bar{r}^2 + \bar{a}^2) + 2\bar{a}^2]^2}, \end{aligned} \quad (\text{A.25})$$

with the common Schwarzschild limit $\mathcal{M}^2 K = -1/\bar{r}^3$. For Kerr it becomes infinite at the threading observer horizon as in the rotating Minkowski case, while remaining finite at the slicing observer horizon (where it vanishes for $\bar{a} = 1$, representing a relatively straight circle). Figure 12 shows the constant ϕ cross-section of the embedding surface for different values of the rotation parameter a in both points of view.

References

1. K. Gödel, *Rev. Mod. Phys.* **21**, 447 (1949).
2. R.P. Kerr, *Phys. Rev. Lett.* **11**, 237 (1963).
3. B. Carter, *Comm. Math. Phys.* **10**, 280 (1968).
4. E.T. Newman, E. Couch, K. Chinnapared, A. Exton, A. Prakash, and R. Torrence, *J. Math. Phys.* **6**, 918 (1965).
5. R.T. Jantzen, P. Carini, and D. Bini, *Ann. Phys. (N.Y.)* **215**, 1 (1992).
6. D. Bini, P. Carini, and R.T. Jantzen, [BCJ1] preprint (1996).
7. W. Rindler and V. Perlick, *Gen. Relativ. Grav.* **22**, 1067 (1990); *errata: Gen. Relativ. Grav.* **23**, 119 (1991).

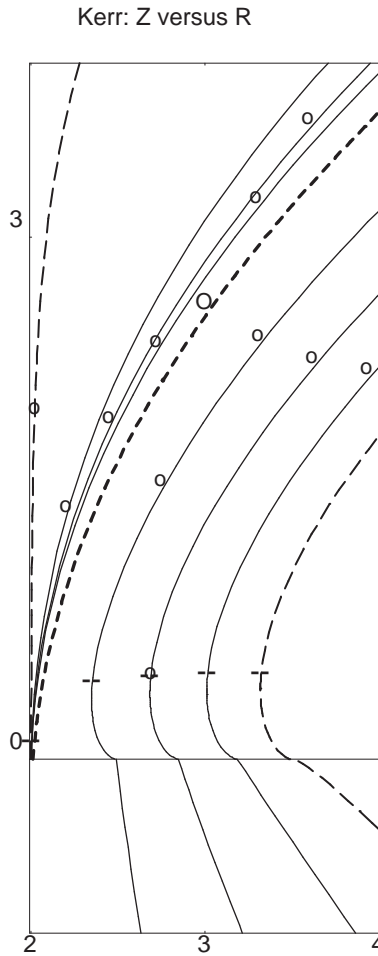


Fig. 12. \bar{Z} versus \bar{R} : embedding cross-section diagrams for the r - ϕ surfaces in both the threading and slicing points of view for the Kerr spacetimes, separated by the thick dashed line at the Schwarzschild case $\bar{a} = 0$. Cross-sections for the Euclidean slicing embedding are shown for the values $\bar{a} = 0, .25, .5, .75, 0.999$ increasing upward above the thick dashed line, while those for the Minkowski threading embedding are below, with the same values increasing downward below, except for the regular final value $\bar{a} = 1$. At nonzero values of \bar{a} , the threading embedding surface starts out at the variable ergosphere outer radius at $R \rightarrow \infty$, moves towards the Z -axis switching signature along the way, and then turns away from the axis at the radius of the single relatively straight circle indicated by a tick mark. The slicing embedding surface starts with a vertical tangent at the horizon $\bar{r} = 2$ for all values of \bar{a} and moves away from the Z -axis, but because the proper distance near the horizon (fixed at $Z = 0$) blows up at $\bar{a} \rightarrow 1$, the interesting part of the embedding diagram is pushed up to infinity.⁵⁵ The circles mark the interface between regions A and B (lower) and then B and C (upper) on each embedding curve, which merge in a single interface at $\bar{a} = 0$ and expand from each other with increasing \bar{a} as in Fig. 4.

8. N.V. Mitskievich, *Relativistic Physics in Arbitrary Reference Frames*, electronic preprint gr-qc/9606051, 1996.
9. D. Bini, P. Carini, R.T. Jantzen, *J. Korean Phys. Soc.* **25**, S190 (1992).
10. D. Bini, P. Carini, and R.T. Jantzen, *Class. Quantum Grav.* **12**, 2549 (1995).
11. M.A. Abramowicz, B. Carter, and J.P. Lasota, *Gen. Relativ. Grav.* **20**, 1173 (1988).
12. M.A. Abramowicz, and A.R. Prasanna, *M.N.R.A.S.* **245**, 720 (1990).
13. M.A. Abramowicz, *M.N.R.A.S.* **245**, 733 (1990).
14. M.A. Abramowicz, in *1989 Summer School in High Energy Physics and Cosmology*, edited by J.C. Pati, S. Randjbar-Daemi, E. Sezgin, and Q. Shafi (World Scientific, Singapore, 1990).
15. M.A. Abramowicz, and J. Bicak, *Gen. Relativ. Grav.* **23**, 941 (1991).
16. M.A. Abramowicz, *M.N.R.A.S.* **256**, 710 (1992).
17. M.A. Abramowicz, J.C. Miller, and Z. Stuchlik, *Phys. Rev.* **D47**, 1440 (1993).
18. A.P. Prasanna, and S.K. Chakrabarti, *Gen. Relativ. Grav.* **22**, 987 (1990).
19. S. Iyer and A.P. Prasanna, *Class. Quantum Grav.* **10**, L13 (1993).
20. M.A. Abramowicz, in *The Renaissance of General Relativity*, edited by G.F.R. Ellis, A. Lanza, and J.C. Miller (Cambridge University Press, Cambridge, 1993).
21. M.A. Abramowicz, P. Nurowski, and N. Wex, *Class. and Quantum Grav.* **10**, L183 (1993).
22. M.A. Abramowicz, P. Nurowski, N. Wex, *Class. and Quantum Grav.* **12**, 1467 (1995).
23. O. Semerák, *Nuovo Cim.* **110B**, 973 (1995).
24. O. Semerák, *Gen. Relativ. Grav.* **28**, 1151 (1996).
25. R. Nayak and C.V. Vishveshwara, *Class. Quantum Grav.* **13**, 1783 (1996).
26. A.P. Prasanna, *Class. Quantum Grav.* **14**, 227 (1997).
27. F. de Felice, *M.N.R.A.S.* **252**, 197 (1991).
28. F. de Felice, and S. Usseglio-Tomasset, *Class. Quantum Grav.* **8**, 1871 (1991).
29. F. de Felice, and S. Usseglio-Tomasset, *Class. Quantum Grav.* **10**, 353 (1993).
30. F. de Felice, *Class. Quantum Grav.* **11**, 1283 (1994).
31. F. de Felice, *Class. Quantum Grav.* **12**, 1119 (1995).
32. F. de Felice, and S. Usseglio-Tomasset, *Gen. Relativ. Grav.* **24**, 1091 (1992).
33. F. de Felice, and S. Usseglio-Tomasset, *Gen. Relativ. Grav.* **28**, 179 (1996).
34. C. Barrabès, B. Boisseau, and W. Israel, *Mon. Not. R. Astron. Soc.* **276**, 432 (1995).
35. B.R. Iyer, and C.V. Vishveshwara, *Class. Quantum Grav.* **5**, 961 (1988).
36. B.R. Iyer and C.V. Vishveshwara, *Phys. Rev.* **D48**, 5721 (1993).
37. E. Honig, E.L. Schücking, and C.V. Vishveshwara, *J. Math. Phys.* **15**, 774 (1974).
38. C.W. Misner, K.S. Thorne and J.A. Wheeler, *Gravitation* (Freeman, San Francisco, 1973).
39. D. Wilkins and M.W. Jacobs, *Phys. Rev.* **D46**, 3395 (1992).
40. R.L. Forward, *Proceedings of the IRE* **49**, 892 (1961).
41. L.D. Landau and E.M. Lifshitz, *The Classical Theory of Fields* (Permagon Press, New York, 1975).
42. J.M. Bardeen, *Astrophys. J.* **162**, 71 (1970).
43. R.D. Greene, E.L. Schücking, and C.V. Vishveshwara, *J. Math. Phys.* **16**, 153 (1975).
44. A. Papapetrou, *Proc. Roy. Soc. London* **209**, 248 (1951).
45. E.J. Post, *Rev. Mod. Phys.* **39**, 475 (1967).
46. A. Ashtekar and A. Magnon, *J. Math. Phys.* **16**, 341 (1975).
47. J. Van Bladel, *Relativity and Engineering*, (Springer-Verlag, Berlin, 1984).
48. R.H. Henriksen and L.A. Nelson, *Can. J. Phys.* **63**, 1393 (1985).
49. S.L. Bazański, preprint (University of Warsaw, Warsaw, 1988).
50. L. Smarr, *Phys. Rev.* **D7**, 289 (1973).
51. K.S. Thorne, in *Quantum Optics, Experimental Gravitation, and Measurement Theory*

- edited by P. Meystre and M.O. Scully (Plenum Press, New York and London, 1981).
52. N.A. Sharp, *Can. J. Phys.* **59**, 688 (1981).
 53. J.D. Romano and R.H. Price, *Class. Quantum Grav.* **12**, 875-894.
 54. I.S. Gradshteyn and I.M. Ryzhik, *Tables of integrals, series and products* (Academic Press, New York, 1980).
 55. K.S. Thorne, R.H. Price, and D.A. Macdonald, *Black Holes: The Membrane Paradigm* (Yale University Press, New Haven, 1986).

Corrections

This reformatted version contains the following misprint corrections of the original article (to which the page numbers refer) and one reference publication update:

- p. 146. Table 1 Line 1: Gödel lapse N change $\sqrt{1-c^2}$ to $\sqrt{1-s^2}$
- p. 147. Eq. (2.3) Line 1: change second minus sign to an equal sign
- p. 150 Table 2. Row for signed relative curvature, Line 2, Gödel (last) column: equal sign missing after kappa symbol before minus sign
- p. 169. Line following Eq. (4.25): change ϕ to $\dot{\phi}$ in both occurrences
- p. 174. Figure 7.(a),(b): The steep downward curve in region B was replaced and the last line of figure caption (a) changed from: “The steep nearly straight curve in region B is . . .”
to
“The curve decreasing from the upper geodesic photon point to the lower geodesic photon point in region B is “. . .”
 $\zeta_{(\text{crit,spin})}$ where the threading precession is extremal.
- p. 176. Eq. (5.4): second subscript “lie” should be in roman type
- p. 182. Eq. (6.16) Line 1: remove γ^2 factor
- p. 188. Eq. (7.10): change 4π to 2π
- p. 189. Eq. (7.12): change $2C(m)$ to $C(m)$